THE GEOLOGICAL SOCIETY OF AMERICA®

Boulders as a lithologic control on river and landscape response to tectonic forcing at the Mendocino triple junction

Charles M. Shobe[1,2,†], Georgina L. Bennett[3], Gregory E. Tucker[1], Kevin Roback[4], Scott R. Miller[5], and Joshua J. Roering[6]

[1]*Cooperative Institute for Research in Environmental Sciences (CIRES) and Department of Geological Sciences, University of Colorado, Boulder, Colorado, USA*
[2]*Helmholtz Centre Potsdam, GFZ German Research Centre for Geosciences, Potsdam, Germany*
[3]*Geography, College of Life and Environmental Sciences, University of Exeter, Exeter, UK*
[4]*Department of Earth and Planetary Sciences, California Institute of Technology, Pasadena, California, USA*
[5]*Department of Geology and Geophysics, University of Utah, Salt Lake City, Utah, USA*
[6]*Department of Earth Sciences, University of Oregon, Eugene, Oregon, USA*

ABSTRACT

Constraining Earth's sediment mass balance over geologic time requires a quantitative understanding of how landscapes respond to transient tectonic perturbations. However, the mechanisms by which bedrock lithology governs landscape response remain poorly understood. Rock type influences the size of sediment delivered to river channels, which controls how efficiently rivers respond to tectonic forcing. The Mendocino triple junction region of northern California, USA, is one landscape in which large boulders, delivered by hillslope failures to channels, may alter the pace of landscape response to a pulse of rock uplift. Boulders frequently delivered by earthflows in one lithology, the Franciscan mélange, have been hypothesized to steepen channels and slow river response to rock uplift, helping to preserve high-elevation, low-relief topography. Channels in other units (the Coastal Belt and the Franciscan schist) may experience little or no erosion inhibition due to boulder delivery. Here we investigate spatial patterns in channel steepness, an indicator of erosion resistance, and how it varies between mélange and non-mélange channels. We then ask whether lithologically controlled boulder delivery to rivers is a possible cause of steepness variations. We find that mélange channels are steeper than Coastal Belt channels but not steeper than schist channels. Though channels in all units steepen with increasing proximity to mapped hillslope failures, absolute steepness values near failures are much higher (~2×) in the mélange and schist than in Coastal Belt units. This could reflect reduced rock erodibility or increased erosion rates in the mélange and schist, or disproportionate steepening due to enhanced boulder delivery by hillslope failures in those units. To investigate the possible influence of lithology-dependent boulder delivery, we map boulders at failure toes in the three units. We find that boulder size, frequency, and concentration are greatest in mélange channels and that Coastal Belt channels have the lowest concentrations. Using our field data to parameterize a mathematical model for channel slope response to boulder delivery, we find that the modeled influence of boulders in the mélange could be strong enough to account for some observed differences in channel steepness between lithologies. At the landscape scale, we lack the data to fully disentangle boulder-induced steepening from that due to spatially varying erosion rates and in situ rock erodibility. However, our boulder mapping and modeling results suggest that lithology-dependent boulder delivery to channels could retard landscape adjustment to tectonic forcing in the mélange and potentially also in the schist. Boulder delivery may modulate landscape response to tectonics and help preserve high-elevation, low-relief topography at the Mendocino triple junction and elsewhere.

INTRODUCTION

The erosional response of landscapes to rock uplift controls topographic relief (Hilley et al., 2019), the longevity of high topography (Egholm et al., 2013), the magnitude and timing of sediment flux to basins (Ding et al., 2019), and the efficiency of geochemical cycling (Ferrier and Kirchner, 2008). The fidelity of the two most accessible records of past changes to Earth's surface—topography and stratigraphy—depends strongly on how landscapes respond to tectonic perturbations. For example, the shape and spatial distribution of "relict" high-elevation, low-relief topography are often used to infer past tectonic forcings, but such topography is ultimately destroyed when landscapes experience changes in tectonic boundary conditions. A quantitative understanding of the factors influencing landscape evolution in transient tectonic settings is critical for deducing past conditions and forecasting future changes to Earth's surface.

River incision into bedrock governs how non-glaciated landscapes respond to transient tectonic perturbations. Under a given tectonic forcing, the major controls on channel evolution are river discharge, sediment flux, caliber, and strength, and the resistance to erosion of the bedrock being incised. Quantitative frameworks have emerged for analyzing the effects of river discharge and its variability (e.g., Tucker and Bras, 2000; Molnar, 2001; Tucker, 2004; Lague et al., 2005; Molnar et al., 2006; Lague, 2014; Deal et al., 2018), sediment flux dynamics (e.g., Sklar and Dietrich, 1998; Whipple and Tucker, 2002; Gasparini et al., 2007; Turowski et al., 2007; Chatanantavet and Parker, 2009; Hobley et al., 2011; Shobe et al., 2017a), and channel geometry adjustment to these two drivers (e.g., Stark, 2006; Wobus et al., 2006a; Lague, 2010; Turowski, 2018; Yanites, 2018).

However, the role of bedrock lithology in governing river erosion and landscape response to tectonics is still poorly understood. The literature is replete with examples of lithologically controlled channel form (e.g., Braun, 1983; Duvall

[†]cshobe@gfz-potsdam.de.

GSA Bulletin; March/April 2021; v. 133; no. 3/4; p. 647–662; https://doi.org/10.1130/B35385.1; 11 figures; 1 supplemental file.
published online 27 July 2020

et al., 2004; Allen et al., 2013; Bursztyn et al., 2015), yet it is often difficult to assign responsibility to a specific control on rock erodibility. These include mineralogical variations (Marshall and Roering, 2014), fracture spacing (DiBiase et al., 2018; Scott and Wohl, 2019), susceptibility to weathering (Johnson and Finnegan, 2015; Murphy et al., 2016; Shobe et al., 2017b), the strength and size of erosive sediment "tools" (Sklar and Dietrich, 1998), and the presence of erosion-inhibiting boulders (e.g., Seidl et al., 1994; Bennett et al., 2016; Shobe et al., 2016; Thaler and Covington, 2016; Cook et al., 2018). We focus here on the role of boulders in changing the pace of river and landscape response in a transient tectonic setting. We adopt an operational definition for what constitutes a boulder: a sediment grain that is likely to remain immobile over geomorphically relevant timescales. In this study we consider boulders to be grains with a long axis length greater than two meters.

The presence of erosion-inhibiting boulders in rivers is partly a consequence of bedrock properties, including mineralogy and fracture spacing. Boulders may be exhumed from the channel floor bedrock or delivered by rockfall, landsliding, and debris flows from adjacent hillslopes. Boulder delivery from hillslopes, at least in steep landscapes, likely dwarfs the number of boulders exhumed from the bed due to the much greater surface area of hillslopes. However, this effect can be counteracted by weathering of hillslope-derived boulders during their journey to the river channel (Sklar et al., 2017; Glade et al., 2019). The presence of boulders has been hypothesized to be a rate-limiting control on river erosion at the reach scale (Gilbert, 1877; Hack, 1965; Howard and Dolan, 1981; Seidl et al., 1994), with confirmation provided by recent field studies (Johnson et al., 2009; Thaler and Covington, 2016; Finnegan et al., 2017; Cook et al., 2018). Modeling results also support the idea that hillslope-derived boulders, by protecting the channel bed and increasing hydraulic drag, steepen channel reaches and inhibit river adjustment to base level fall under common boulder size and hydrologic scenarios (Shobe et al., 2016; Shobe et al., 2018; Glade et al., 2019). Boulder delivery to channels may be one important way in which lithological heterogeneity leaves its imprint on the landscape and governs the response of Earth's surface to transient tectonic perturbations.

Despite recent progress at the channel-reach scale (Johnson et al., 2009; Thaler and Covington, 2016; Finnegan et al., 2017), little evidence exists for how lithology-dependent boulder delivery influences transient landscapes. DiBiase et al. (2018) analyzed portions of two individual mountain ranges with similar lithology and discharge distributions under approximate steady-state erosion conditions and found that fracture density correlates with channel and landscape steepness. They interpreted this correlation as reflecting an increased load of coarse sediment delivered to rivers when fractures are widely spaced. In another recent study, which we expand upon in this paper, Bennett et al. (2016) investigated landscape response to tectonic forcing in the Mendocino triple junction region of California. They proposed a lithologic control on boulder delivery and landscape morphology following hypotheses developed by Kelsey (1978). Bennett et al. (2016) theorized that channels are steeper and more completely mantled with boulders in the mechanically weak Franciscan mélange than the possibly more competent rock of the nearby Franciscan schist and Coastal Belt. They hypothesized that large boulders, delivered to rivers by earthflows (large, slow-moving landslides), steepen channels and inhibit landscape adjustment preferentially in the mélange. However, Bennett et al. (2016) did not explicitly test for boulder delivery as a lithologic control on channel and landscape form.

One substantial challenge when analyzing controls on channel steepness in a transient landscape is disentangling grain size controls from the effects of (1) the intrinsic (in situ) rock erodibility, independent of grain size, and (2) variable erosion rates, in this case triggered by complex patterns of rock uplift in the Mendocino triple junction region. Attempting to constrain the influence of lithology-dependent boulder delivery on channel and landscape evolution is important in spite of these complications, given that boulder delivery could alter landscape form and adjustment dynamics over geologic timescales both in the Mendocino triple junction region and in other landscapes (e.g., Seidl et al., 1994; Glade et al., 2019).

In this paper, we study the Mendocino triple junction region (Fig. 1) to further investigate the idea that earthflow-derived boulders in the Franciscan mélange influence channel form and landscape evolution. We address three questions:

(1) Are there distinct differences in river channel form between the Franciscan mélange and other units?

(2) Are changes in channel form correlated with proximity to hillslope failures, and do those hillslope failures preferentially deliver boulders to mélange channels?

(3) What is the expected magnitude of channel steepening given the boulder size distributions found in mélange channels?

To address (1) and (2) we conduct morphometric analyses of the Mendocino triple junction landscape and map the size distributions of boulders delivered to channels by hillslope failures across the three main mapped units (Franciscan mélange, Franciscan schist, and Coastal Belt). We then introduce a numerical model for river erosion in the presence of boulders to address (3).

STUDY AREA

The study area covers four basins draining the northern California coast range: the Russian, Eel, and Mad Rivers and Redwood Creek (Fig. 1B).

Geodynamic and Tectonic Setting

The study area is responding to a transient wave of rock uplift due to tectonic and geodynamic activity at the Mendocino triple junction, the meeting point of the North American, Pacific, and Gorda tectonic plates. Geodynamic modeling suggests that the Mendocino triple junction is causing a northward-migrating zone of rapid rock uplift due to crustal thickening, followed by a zone of subsidence due to crustal thinning (Furlong and Govers, 1999). Crustal thickening and thinning are thought to result in local rock uplift rates of up to 2 mm/yr and down to −2 mm/yr (Lock et al., 2006). These rates are broadly consistent with those determined from the altitudinal spacing of nearby marine terraces (Merritts and Bull, 1989). Mean values may represent rock uplift rates that are stochastic in time, as major rock uplift events may have occurred due to large magnitude earthquakes (Merritts, 1996). The northward migration of the zones of thickening and thinning over the past ca. 8 Ma results in a pattern of cumulative rock uplift with an expected peak in the upper Eel River basin and subsidence predicted farther north and south (Furlong and Govers, 1999; Lock et al., 2006; Bennett et al., 2016).

Regional Erosion Rates

Past studies have found patterns of erosion consistent with the proposed geodynamic forcing. While mainstem channels in small coastal drainages are thought to be adjusted to the tectonic forcing (Merritts and Vincent, 1989; Snyder et al., 2000), low-order tributaries and hillslopes may remain in a state of transient response even after mainstem channels have adjusted (Moon et al., 2018). Knickpoints are prevalent on river profiles in the Eel River basin (Foster and Kelsey, 2012; Willenbring et al., 2013; Bennett et al., 2016), indicating that erosion rate measurements from small coastal basins may be of limited relevance further inland. Cosmogenic nuclide concentrations in river sediment in the Eel River basin suggest that erosion rates are highly variable in space (Balco et al., 2013; Willenbring

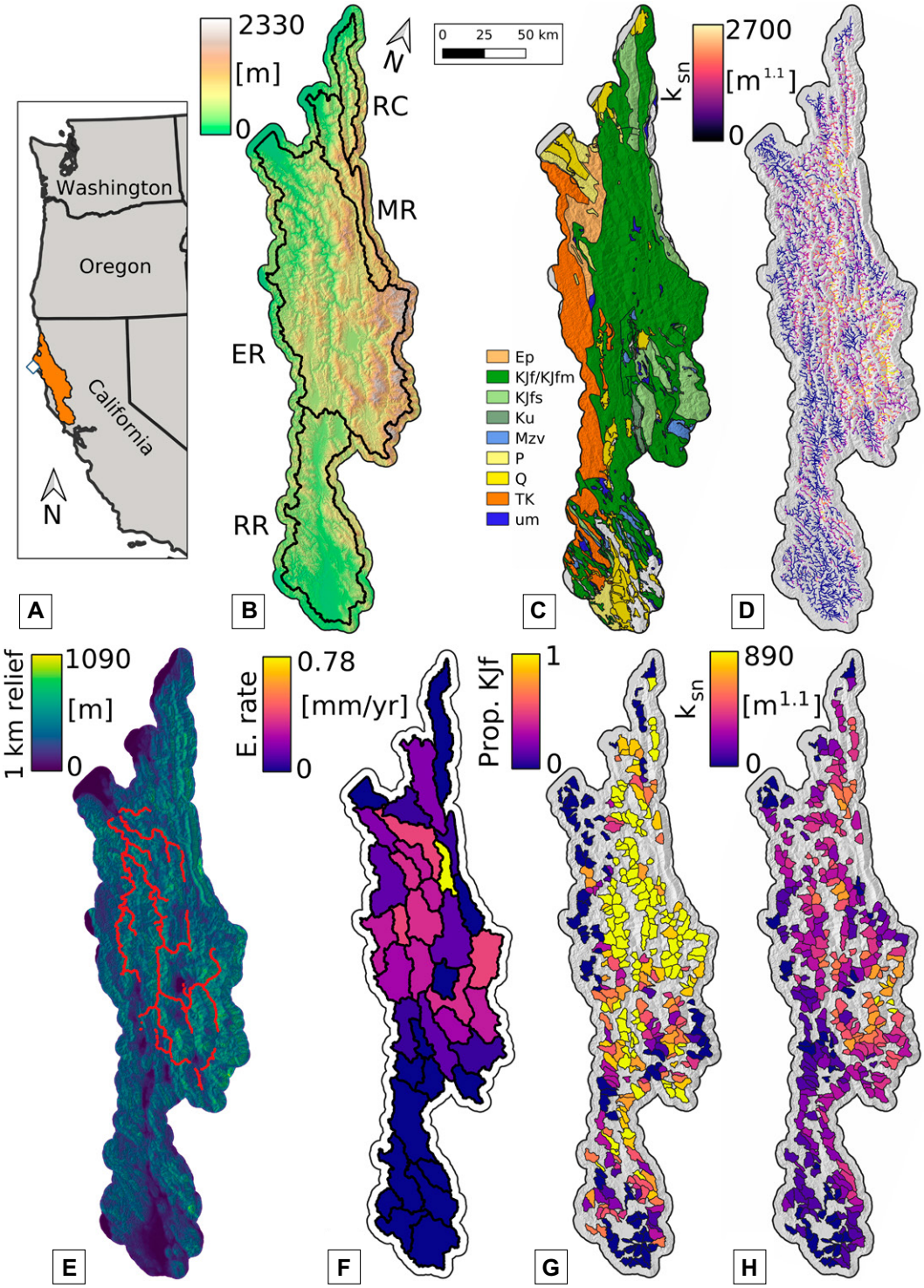

Figure 1. (A) Study area location in coastal California, USA (orange region). White diamond shows the location of the Mendocino triple junction. (B) Shown is a 10 m Digital Elevation Model (DEM) overlain with the boundaries of the four major drainage basins: the Russian River (RR), the Eel River (ER), the Mad River (MR), and Redwood Creek (RC). (C) Geologic map of the study area after Jennings (1977). Ep—Paleocene sandstones and mudstones; KJf/KJfm—Jurassic to Cretaceous Franciscan mélange; KJfs—Early Cretaceous Franciscan schist; Ku—Late Cretaceous sandstones; Mzv—Jurassic to Cretaceous basalt; P—Miocene to Pleistocene sandstones; Q—Quaternary sediments; TK—Late Cretaceous to Pliocene sandstones and mudstones; um—ultramafic rocks. See text for further description of relevant rock units. (D) Normalized channel steepness indices from Bennett et al. (2016). (E) Local relief calculated in a 1 km moving window. Red points indicate the locations of 986 channel width measurements made in Google Earth. (F) The 38 subcatchments used for analysis of erosion rate-channel steepness relationships by Bennett et al. (2016) are shown, colored by landslide erosion rate. In this study, we used 344 subcatchments of uniform drainage area (10–50 km^2) that we delineated following Forte et al. (2016). Here we show those subcatchments colored by (G) proportion of the subcatchment underlain by Franciscan mélange and (H) catchment-averaged channel steepness.

et al., 2013; Roering et al., 2015). Geologic evidence exists for drainage divide migration in response to spatially variable rock uplift (Lock et al., 2006). Overall, there is evidence for significant landscape transience in our study area due to the complex geodynamic forcing. However, Bennett et al. (2016) demonstrated that erosion rate measurements from landslide mapping show a pattern that is broadly similar to the cumulative rock uplift predicted by the geodynamic modeling of Furlong and Govers (1999). Clubb et al. (2020) inferred the same rock uplift pattern from analysis of channel and hillslope geometry in the region. This indicates that while erosion rates vary in space, landscape form is broadly reflective of the rock uplift forcing.

Lithology

Two broad geologic map units underlie the study area: the Coastal Belt and Central Belt of

the Franciscan Complex. The Franciscan Complex is a mix of metamorphosed marine sediments that was accreted to the North American plate during subduction of the Farallon plate (Mclaughlin et al., 2000), and it exhibits significant spatial heterogeneity in rock type. All geologic map information used in this study was derived from the geologic map of California (Jennings, 1977).

The Central Belt of the Franciscan Complex contains two key units. The first, which we refer to as the Franciscan mélange and define as being the mapped units KJf and KJfm (Fig. 1C), is a mélange of sedimentary and metasedimentary rocks primarily composed of graywacke and sheared mudstone. These two units are sometimes mapped together as KJf (Jennings, 1977) such that separating the two units would not be meaningful. The mélange also contains gabbro sills and dikes, as well as boulders of serpentinite, greenstone, and amphibolite within the graywacke and mudstone matrix. The second unit of the Central Belt in our study area, the Franciscan schist, is mapped as KJfs. The schist is a strongly deformed blueschist that also contains more minor occurrences of metasandstone and metagraywacke. We analyze the schist unit separately from the other Central Belt units (KJf and KJfm) because we expect substantial contrasts in in situ rock strength between the mélange and the schist, potentially causing channel steepness differences unrelated to boulder delivery. The Central Belt has a few spatially restricted occurrences of Mesozoic ultramafic rocks (um).

The Coastal Belt is chiefly composed of the Yager terrane (mapped Ep), a Paleocene to Eocene mix of argillite, sandstone, and conglomerate, and the Coastal terrane (mapped TK), a more pervasively sheared unit of sandstone, shale, and minor conglomerate. The Coastal terrane also contains minor amounts of Jurassic to Cretaceous basalts (Mzv) and ultramafics. While we expect significant rock strength contrasts between the sedimentary rocks and the basalts and ultramafics, the extents of the latter two are spatially restricted (Fig. 1C) and unlikely to influence our landscape-scale analysis. From here on we refer to all units besides the mélange (KJf/KJfm) and schist (KJfs) as non-KJf units.

The lithologic differences between the mélange and the Coastal Belt are associated with diagnostic differences in the types of hillslope failures observed. Earthflows, slow-moving landslides that predominantly undergo displacement along a basal failure plane as well as internal shear deformation, are common in the mélange (Kelsey, 1978; Keefer and Johnson, 1983; Iverson and Major, 1987; Mackey and Roering, 2011; Hungr et al., 2014; Handwerger et al., 2015; Bennett et al., 2016; Nereson and Finnegan, 2019). In contrast, hillslopes in the Coastal Belt fail in debris slides, which tend to be smaller, shallower, faster granular slides (Hungr et al., 2014; Bennett et al., 2016). While the mélange experiences both earthflows and debris slides, there are very few earthflows in the non-KJf units. The schist predominantly experiences debris slides, but some earthflows are also observed.

Sediment and Bedrock Exposure in Mendocino Triple Junction Rivers

Rivers draining the study area (Fig. 2) are characterized by high sediment loads due to a combination of rock uplift relative to base level, weak rock in large portions of the region and a flood-dominated hydrologic regime (Syvitski and Morehead, 1999) that drives hillslope sediment delivery as well as river discharge (Kelsey, 1980). Human modifications to the basins have likely increased fluvial sediment loads in recent times (Kelsey, 1980). While the rock uplift rates deduced from geodynamic models (Furlong and Govers, 1999) and geomorphic analyses (Bennett et al., 2016; Clubb et al., 2020) suggest that channels in the region must incise bedrock over geologic timescales, many river reaches exhibit partial to near-complete sediment cover even in steep reaches such as the major knickzone on the South Fork Eel River (Foster and Kelsey, 2012; Fig. 2B). We observe some bedrock exposed in the steepest channels regardless of lithology, but bedrock exposure is almost never complete. The grain size of in-channel sediment is highly spatially variable, especially in the mélange and schist channels (Figs. 2A and 2C). Grain size variability may result from heterogeneity in the rock itself and/or concentration of large grains in channels by hillslope failures (Finnegan et al., 2019).

Previous Work on Lithologic Control over Mendocino Triple Junction Landscape Form

The idea that lithology may play an important role in governing landscape response to tectonic forcing at the Mendocino triple junction is not new. Kelsey (1978) noted that earthflows seem to be most prevalent in the mélange and suggested that large boulders delivered by earthflows to channels armor the channel bed and force earthflow-bound channels to steepen. Extrapolating Kelsey's ideas to the landscape scale results in the prediction that all else being equal, channels in the mélange might be steeper than their non-mélange counterparts for a given erosion rate due to the delivery of erosion-inhibiting, earthflow-derived boulders.

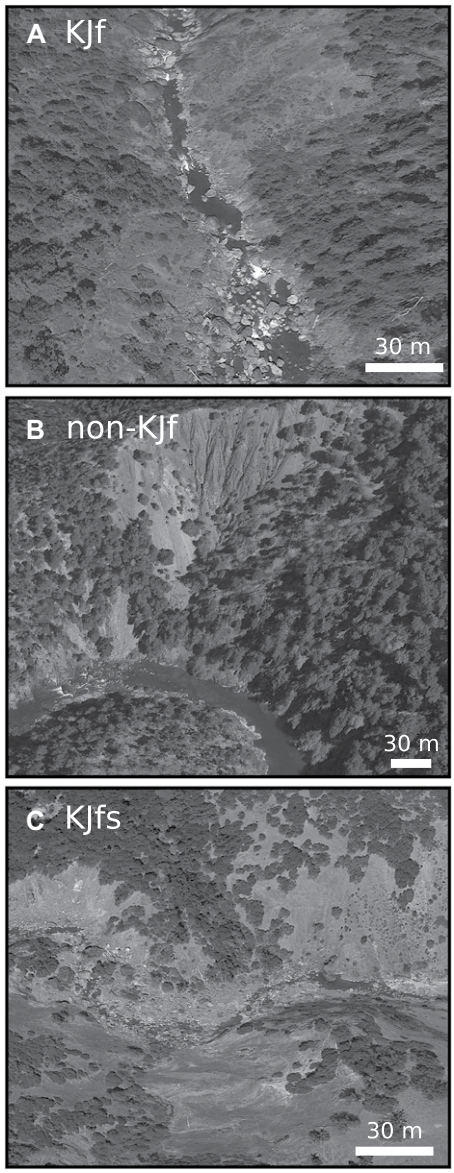

Figure 2. Google Earth images showing rivers incising (A) the Franciscan mélange, (B) the Coastal Belt, and (C) the Franciscan schist. All images show channel reaches at the toe of hillslope failures mapped by Bennett et al. (2016). Boulder mapping indicates that dimensionless boulder concentrations are greater in A and C than in B (locations are marked on Fig. 10). Image dates and locations can be found in the supporting information.

Recently, Finnegan et al. (2019) analyzed sites in the mélange where earthflows impinge on river channels to explore channel response to the delivery of large, earthflow-derived boulders. They showed examples of earthflow-influenced channel longitudinal profiles within the mélange and described two possible resulting channel

morphologies: (1) a steep lip or knickpoint representing the downstream edge of a valley-blocking deposit of "jammed," earthflow-derived boulders (observed in channels with low drainage area and width) and (2) a reach experiencing earthflow sediment delivery but whose steepness was not significantly affected (observed in larger channels). These results suggest that boulder-induced steepening may occur in the mélange, if only in a subset of channels prone to jamming—i.e., where channel width is small relative to the seasonal displacement of boulder-delivering earthflows. This study highlights that there are two possible, non-exclusive mechanisms of channel steepening: creation of a knickpoint lip by boulder delivery and valley blocking, and longer-term adjustment of the underlying bedrock surface through preferential erosion in locations not mantled with boulders (e.g., Shobe et al., 2016). Both mechanisms imply a reduction in the average efficiency of river erosion due to boulder delivery by earthflows. Valley blocking that persists sufficiently long would lead to adjustment of the bedrock surface.

As discussed above, analysis of landslide erosion rates and channel steepness led Bennett et al. (2016) to suggest that earthflow-derived boulders may preferentially steepen channels in the mélange relative to the Coastal Belt and schist. They divided their study area (the same as ours) into 38 subcatchments and compared mean landslide erosion rates (Fig. 1F) with mean channel steepness for each subcatchment. We present their data in Figure 3A, with points shaded to represent the proportion of each subcatchment's area underlain by mélange. These data are equivocal about the existence of a lithologic control on landscape form. The relationship between erosion rate (E) and steepness index (k_{sn}) in the study area is relatively well-described by a power-law relationship with a power $\varphi < 1$ (Fig. 3):

$$k_{sn} = E^{\varphi} \quad (1)$$

where k_{sn} is the normalized channel steepness index (slope normalized by drainage area), defined as

$$k_{sn} = \frac{S}{A^{-\theta_{ref}}}. \quad (2)$$

S is channel slope, A is drainage area, and θ_{ref} is a reference concavity index (Whipple and Tucker, 1999) whose value is discussed below. This type of power-law relationship between erosion rate and channel steepness with $\varphi < 1$ is expected in drainage basins that experience a spatially constant, non-negligible erosion threshold (e.g., Tucker, 2004; Lague et al., 2005; DiBiase and Whipple, 2011) due to the lessening importance of the threshold at greater erosion rates even in the absence of a lithologic control on channel steepness. Snyder et al. (2003a, 2003b) found a relationship of similar form to Figure 3A for the relationship between rock uplift rate and channel slope for coastal drainages in the Mendocino triple junction region.

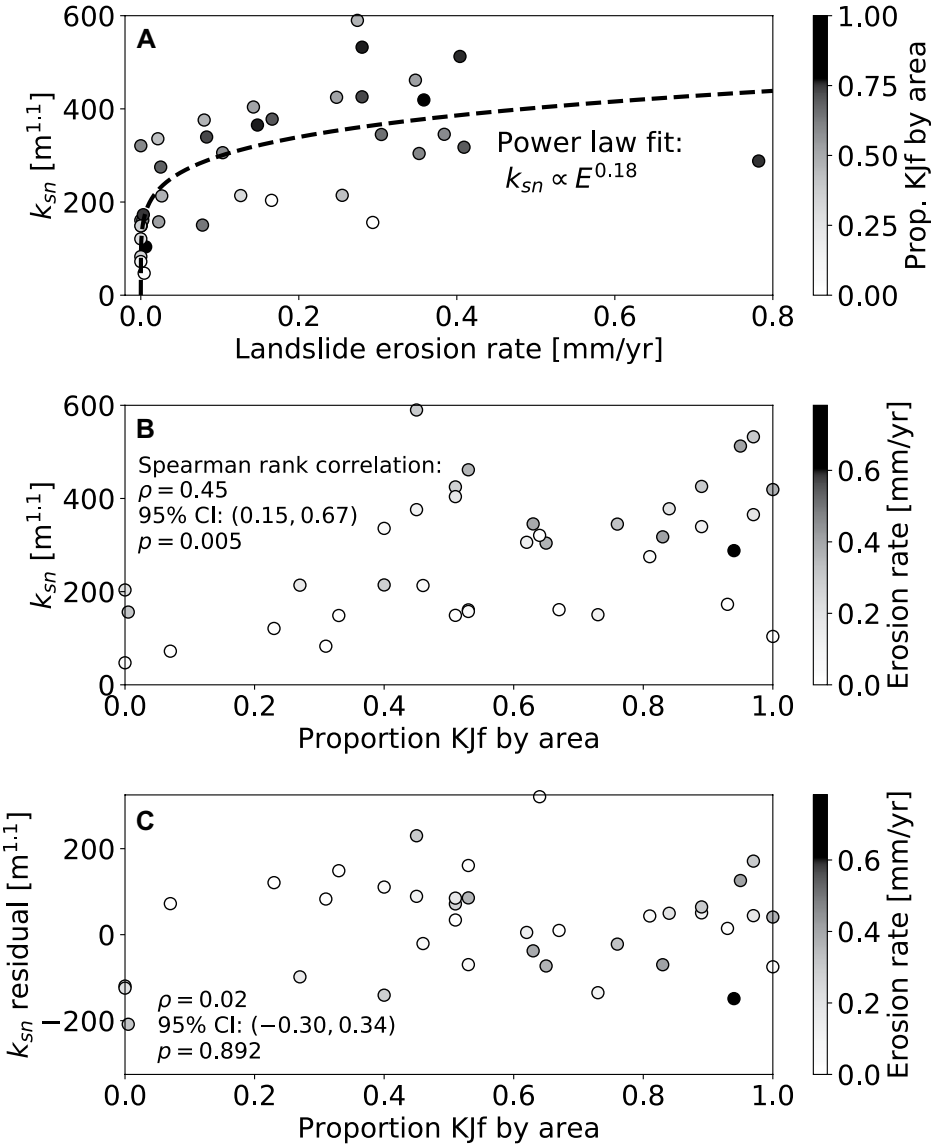

Figure 3. (A) Catchment-averaged channel steepness for 38 subcatchments shown as a function of catchment-averaged landslide erosion rate. (B) Catchment-averaged channel steepness shown as a function of the proportion of subcatchment underlain by Franciscan mélange rock. A Spearman correlation test shows a statistically significant correlation between proportion of mélange underlying a given subcatchment and its mean channel steepness. (C) Residuals from the fit in (A) plotted as a function of the proportion of each subcatchment underlain by mélange rock. There is no significant correlation between proportion of mélange and deviation from the power-law fit. All data in this figure are from Bennett et al. (2016). CI—confidence interval.

Plotting the subcatchment-averaged channel steepness as a function of the proportion of a subcatchment underlain by mélange (Fig. 3B) shows that steepness is significantly correlated ($p = 0.005$) with increasing proportion of mélange underlying a basin. However, plotting residuals from the fit in Figure 3A as a function of basin lithology (Fig. 3C) to remove the effects of changing erosion rate shows no significant correlation ($p = 0.892$) between proportion of mélange and deviation from the power-law erosion rate-channel steepness relationship. This could suggest that lithology may not strongly

influence landscape form once erosion rate variations are accounted for, but does not account for the potentially differing influences of the non-KJf units and the schist, which were not separated in Bennett et al.'s (2016) analysis. Perhaps most importantly, there are currently no data sets of boulder delivery to channels in the different rock units in the Mendocino triple junction region. The existence and influence of lithology-dependent boulder delivery in this landscape are open questions.

Here we investigate how the propensity of a lithology to deliver boulders to river channels—for example, by hillslope failures—might influence river and landscape response to Mendocino triple junction tectonics. While we focus on the Mendocino triple junction as a test case because of the large amount of available data and previous work in this region, our analysis applies to any landscape in which lithology, by controlling sediment size, might govern transient landscape adjustment (e.g., Thaler and Covington, 2016; Finnegan et al., 2017; DiBiase et al., 2018; Glade et al., 2019).

METHODS

We first analyzed channel steepness and width indices and their relationship to mapped bedrock lithology, with the goal of exploring how steepness and width change with underlying rock type. We then delineated 344 headwater subcatchments and tested the relative influence of mélange, Coastal Belt, and schist occurrence on mean channel steepness. Because boulders are thought to be delivered to mélange channels by hillslope failures, we analyzed the potential influence of proximity to the nearest hillslope failure on channel steepness and width in the mélange, the Coastal Belt, and the schist. We mapped boulder size distributions at the toes of hillslope failures in all three units to assess differences in boulder delivery to channels among the units. Finally, we used our boulder mapping data to parameterize a numerical model for channel steepening in the presence of boulders.

Lithology

We derived all lithologic information from the publicly available geographic information system (GIS) layers for the geologic map of California (Jennings, 1977). Following Bennett et al. (2016), we considered anything mapped as KJf or KJfm to be the Franciscan mélange (Fig. 1C). The Franciscan schist (KJfs) was treated as a separate unit because it does not contain abundant earthflows (Bennett et al., 2016) and may have substantially different mechanical properties from the KJf and KJfm (Jennings, 1977; Roadifer et al., 2009). We used the geologic map to extract the proportion of each headwater subcatchment underlain by the mélange (Fig. 1G), non-KJf units, and the schist, as well as to assign a lithology to each channel steepness and width measurement.

Channel Steepness and Width Indices

The normalized channel steepness index is a measure of channel slope normalized by drainage area and is calculated using Equation 2. In this case, S is local slope smoothed over a moving window, and θ_{ref} is a reference concavity representing the mean concavity of channels in the study region. Steeper channels are thought to indicate either more rapid erosion or reduced erodibility. We used the normalized channel steepness data set presented by Bennett et al. (2016). They used Topotoolbox 2 (Schwanghart and Scherler, 2014) on the 10 m National Elevation Data set (NED) digital elevation model (DEM). They filtered the channel elevations with a 100 m moving window filter to remove noise from the DEM (Wobus et al., 2006b), then calculated normalized steepness indices using a 1000 m moving window and a reference concavity of $\theta = 0.55$, calculated by Shi (2011) for the study area. This procedure resulted in 102,303 channel segments, each with a normalized steepness index. We calculated the center point of each channel segment and used the center point to determine on which lithologic unit the segment was located. If a channel segment crossed a geologic contact, the unit on which the centerpoint lay was assigned to that segment. All channel steepness measurements are shown in Figure 1D.

We mapped 986 channel widths for channels with drainage area > 100 km^2 from 0.3 m resolution basemap imagery (ESRI World Imagery, in which data for the continental United States is derived from DigitalGlobe imagery). Widths were measured at intervals of 1 km along the river network and in several additional locations selected to include channels at the base of active earthflows. Width measurements were made by drawing a line from bank to bank perpendicular to the direction of flow. We did not measure widths in places where confident channel bank identification was not possible. Examples of channels not measured include channels partially or fully covered by overhanging vegetation, channels whose banks were cast into shadow in the imagery by nearby steep topography, and channels that were split into multiple threads at the point of measurement. We did not take width measurements of channels that were so choked with boulders that banks could not be identified. This has the potential to influence our study by excluding the most heavily boulder-influenced channels, but because we measured the width of large channels, very few channels were so choked with boulders (Finnegan et al., 2019) that widths could not be measured. Measurement locations for channel width are shown in Figure 1E.

We calculated a channel width index for each width measurement to remove the effects of drainage area. Normalized width indices are calculated by:

$$k_{wn} = \frac{w}{A^b}, \tag{3}$$

where w is measured channel width, A is drainage area, and b is the power governing the relationship between drainage area and measured width (Yanites and Tucker, 2010; Allen et al., 2013). For our study region, we found $b = 0.4$. As we did for channel steepness segments, we calculated the center point of each flow-perpendicular channel width line segment to determine which lithologic unit the width measurement overlay.

Subcatchment Delineation

Understanding the influence of lithology on landscape-scale channel morphology requires the definition of some spatial scale over which channel steepness can be averaged. Because the drainage network communicates transient signals through landscapes, delineating headwater subcatchments increases the likelihood that channels experiencing the same erosion rate forcing are averaged together. Subcatchments should contain channels of similar drainage area so that the effects of changing drainage area are not convolved with channel steepness averages. Following Forte et al. (2016), we divided our study area into subcatchments of similar drainage area so that quantities such as channel steepness index could be averaged over a defined spatial scale and compared against the lithologic makeup of each subcatchment. We used the 10 m resolution NED DEM and delineated subcatchments using flow routing tools available through GRASS GIS (GRASS Development Team, 2018). We imposed that subcatchments would have minimum and maximum drainage areas of 10 km^2 and 50 km^2 respectively, and in every case we extracted the largest possible subcatchment < 50 km^2. This procedure resulted in 344 individual subcatchments well-distributed throughout the study area (Figs. 1G and 1H) and differs from the analysis of Bennett et al. (2016) in that channel segments were only grouped with others of similar drainage area.

Channel Proximity to Hillslope Failures

To investigate the effects of proximity to hillslope failures on channel morphology across

lithologic units, we calculated the straight-line distance from each channel segment center point (for both steepness and width measurements) to the nearest point on the edge of the nearest hillslope failure using the GRASS GIS "v.distance" tool (GRASS Development Team, 2018). We used the data set of mass movements presented by Bennett et al. (2016), which includes 2320 active earthflows, dormant earthflows, and debris slides. In addition to analyzing distance to failure as a continuous data set, we separated channel steepness and width measurements into two groups: those that were within 100 m of the nearest hillslope failure and those that were farther than 100 m from the nearest failure. We also tested values of 25 m, 50 m, and 200 m for the distance cutoff but found no significant differences in the results. While straight-line distance is only intended to be a rough predictor of whether or not a channel segment might be influenced by any specific hillslope failure (for example, the failure may not have its toe at the channel or the channel reach may be upstream of the failure), it is an indicator of whether a channel is receiving substantial sediment delivery from hillslope failures over geologic time.

Boulder Mapping

We used imagery available through the Google Earth application to map the in-channel deposits at the toes of channel-adjacent hillslope failures. This allowed us to determine the size and quantity of boulders delivered to channels in each of the three lithologies. We randomly selected failures in the mélange and schist units and then skipped failures not connected directly to a channel or where vegetation obscured the channel bed. This approach resulted in a sample encompassing more channels at large drainage area than headwater channels, because headwater channels were more frequently obscured by vegetation. In the non-KJf we mapped boulders at hillslope failures in the South Fork Eel River knickzone due to a lack of large, channel-adjacent debris slides elsewhere in the unit. This sample should encompass the failures with the greatest boulder delivery and thereby yield maximum boulder counts and concentrations for the non-KJf.

We mapped boulders by exporting Google Earth images with a vertical view angle and an eye height of ~200 m to the image analysis program ImageJ (version 1.52a, Rasband, 2019). Using ImageJ, we used the scale bar from Google Earth to define a ratio of image pixels to meters and then mapped and calculated the long axis length of every boulder visible in each photograph. We did not attempt to map submerged boulders. We used a minimum boulder size of 2 m in our analysis for two reasons. First, boulders much smaller than 2 m are more likely to be frequently mobile (Finnegan et al., 2019) and therefore do not resist erosion through long-term increases in bed cover and hydraulic roughness. Second, we found that the ability to distinguish among boulders, deposits of smaller sediment grains, and bedrock became substantially worse as we attempted to map boulders of sizes approaching 1 m in the imagery.

To account for the effects of measurement area size, we calculated a dimensionless boulder concentration N_b for each site:

$$N_b = \frac{\Sigma D_i^2}{LW}, \tag{4}$$

where D_i is the measured long axis length of each boulder, L is the length of the channel along which boulders were mapped, and W is the width of the measurement area. The more boulders > 2 m mapped in a reach of a given size, or the larger the boulders, the higher the N_b value for the reach. Because our goal was to capture the occurrence and size of all boulders being delivered to the channel, the width of our measurement area often extended up the channel banks past the waterline. While squaring the long axis length D provides an overestimate of total boulder area per unit channel area, we use N_b only as a way of comparing sites against one another and not to establish a true estimate of the volume of rock in the channel. We mapped 10 images in each of the three rock units. Those 10 images spanned six earthflow toes (in the KJf; earthflow toes were often longer than a single image could capture), 10 debris slide toes (in the non-KJf), and 10 failures including a mix of earthflows and debris slides (in the KJfs). Locations where boulders were mapped are listed in the Data Repository[1] for this article. Images used for mapping are available in a permanent repository (Shobe et al., 2020).

Numerical Model for Boulder-Induced Channel Steepening

We use theory from previous work (Shobe et al., 2016, 2018; Glade et al., 2019) to develop a steady-state model for how a channel reach responds to the presence of boulders. The model seeks to answer the question: how much would a boulder-mantled channel reach need to steepen relative to a channel with no boulders to achieve a given erosion rate? The model is zero-dimensional; it represents a patch of channel bed with a given discharge, channel width, number of boulders, and mean boulder size. The key feature of the model, the full details of which can be found in Shobe et al. (2016, 2018), is a modified shear stress erosion rule that takes into account both the effects of bed cover by boulders and hydraulic drag increases caused by the presence of boulders. In this simple model, boulders are assumed to be immobile, an assumption relaxed by Shobe et al. (2016, 2018). The model assumes a constant effective water discharge for simplicity. The vertical bed lowering rate E is calculated as:

$$E = k\frac{\rho g h S}{1+\sigma_D}\left(1 - f_c\right), \tag{5}$$

where k is an erodibility constant that is unaffected by the presence of boulders, ρ is water density, g is acceleration due to gravity, h is flow depth, and S is channel slope. f_c is the fraction of the bed covered by boulders and σ_D is the dimensionless drag stress caused by the presence of boulders (Smith, 2004; Kean and Smith, 2004, 2010). When no boulders are present in the channel (i.e., σ_D and f_c are both zero), Equation 5 simplifies to the well-known shear-stress approximation for river erosion (e.g., Howard, 1994). With boulders in the channel, the dimensionless drag stress is given by:

$$\sigma_D = \frac{1}{2} C_D \beta^2 \frac{H_b D}{\lambda^2}, \tag{6}$$

where C_D is the drag coefficient (set to a constant value of 1.0 for a cube in a flow), H_b is the average depth to which boulders are submerged, D is average boulder long axis length, and λ is the average spacing of boulders (Smith, 2004; Kean and Smith, 2004, 2010). β is a dimensionless roughness coefficient that we obtain by solving the Variable Power flow resistance equation (Ferguson, 2007), which has been shown to be an effective resistance relation for flows with high relative roughness. The presence of boulders in the model affects the flow depth h according to the formulation of Kean and Smith (2010):

$$h = \frac{q}{u} = q \Big/ \left(\sqrt{\frac{ghS}{1+\sigma_D}}\beta\right), \tag{7}$$

where q is the imposed discharge per unit width. Equation 7, coupled with the flow resistance equation (in which h enters the problem again), is solved numerically. This approach extends the model of Shobe et al. (2016, 2018), who did not explicitly calculate the influence of boulders on flow depth-velocity partitioning. The cover

[1]Supplemental Material. Boulder mapping locations. Please visit https://doi.org/10.1130/GSAB.S.12515336 to access the supplemental material, and contact editing@geosociety.org with any questions.

fraction f_c is calculated using the boulder sizes and counts derived from our boulder mapping.

The model is solved to compare two cases, a channel reach with no boulders and a reach with boulders, by assuming that the channel will adjust its slope to attain the same imposed erosion rate regardless of the presence of boulders. This implies that boulder supply must be consistent enough over the timescale of channel slope adjustment to maintain a given concentration of boulders in the channel, a condition which is likely met in our study area as hillslopes maintain threshold angles by landsliding in response to continued rock uplift (Bennett et al., 2016). If erosion rates are equal between a boulder-free reach (E_i) and a boulder-mantled reach (E_b) such that:

$$E_i = E_b, \tag{8}$$

then the lack of boulder-induced drag stress and bed cover in the boulder-free reach implies that:

$$k\rho g h_i S_i = k\frac{\rho g h_b S_b}{1+\sigma_D}\left(1-f_c\right). \tag{9}$$

Here h_i and h_b denote the flow depths (and S_i and S_b the channel slopes) of the two reaches of equivalent erosion rate: the boulder-free reach and the boulder-mantled reach, respectively. Boulders change flow depth by increasing hydraulic drag and by causing channel steepening that further alters the partitioning between flow depth and velocity.

We can solve Equation 9 for the channel slope of the boulder-mantled reach relative to the boulder-free reach. This is a measure of how much steeper the boulder-mantled channel would need to be, for a given mean boulder size D and spacing λ, to achieve the same erosion rate experienced by a boulder-free channel reach with the same discharge and channel width. The steepening ratio S_b/S_i is found by:

$$\frac{S_b}{S_i} = \frac{\left(1+\sigma_D\right)h_i}{\left(1-f_c\right)h_b}. \tag{10}$$

By combining Equations 6, 7, 10, and Ferguson's (2007) Variable Power flow resistance equation, we can solve for the unique combination of boulder-mantled channel slope S_b, boulder-mantled channel flow depth h_b, and dimensionless drag stress σ_D that produces an erosion rate identical to that for the boulder-free channel reach (left side of Equation 8 and 9). The outcome of interest is the channel steepening due to boulders, S_b/S_i.

We use the boulder size and occurrence information derived from our boulder mapping to parameterize this model and explore the likely range of channel steepening in our study area. Three key assumptions underlie the model calculations. The first is that the boulders of average long axis length D do not move under the slope and discharge conditions in the model. Our model no longer applies once the channel reach steepens to the point where boulders of size D are mobile. The second assumption is that channel width does not adjust to boulder-induced channel steepening. There is mixed field evidence for whether channel width variations accompany changes in slope under uniform erosion rates (Duvall et al., 2004; Whipple, 2004). Further, width dynamics may depend on sediment flux (Yanites, 2018), an unconstrained variable in our study. The third assumption is that the imposed discharge per unit width q is representative of the discharge distribution across the study area. The flood-prone nature of the Mendocino triple junction region (Syvitski and Morehead, 1999) and the considerable variation in mean annual precipitation across the study area (~889 mm to ~2540 mm; Brown and Ritter, 1971) make the discharge distribution a topic worthy of future investigation. However, because our goal is to isolate the effects of boulders, we hold discharge constant (though we test two different mean discharge values; see Results and Discussion).

RESULTS AND DISCUSSION

Lithology, Channel Steepness, and Channel Width

We present density plots showing the distribution of channel steepness indices across the three main lithologic groups (Fig. 4): the mélange (KJf), the schist (KJfs), and all other lithologies (non-KJf). Density plots were created using the seaborn Python library with a Gaussian kernel. The lithology with the greatest mean channel steepness (395 $m^{1.1}$) is the schist, followed by the mélange (352 $m^{1.1}$). The non-KJf channels have by far the lowest mean channel steepness (152 $m^{1.1}$). Note that there are no steepness index values below zero; any values plotting below zero are an artifact of the kernel density estimator. A Kruskal-Wallis H-test suggests that the three populations are not all drawn from the same distribution ($p < 0.001$). We conducted post-hoc Dunn's tests for each pairing, with corrections for multiple comparisons using the Holm method, to determine which populations were significantly different from one another. Each is significantly different from the others ($p < 0.001$). All statistical tests in this paper used the pingouin statistics package (Vallat, 2018), the scikit-posthocs statistics package (Terpilowski, 2019), and/or the scipy.stats package for Python.

Channel width differences among the three lithologies do not follow the same pattern as the differences in steepness (Fig. 5). The non-KJf channels show the greatest mean width index (0.0075 $m^{0.2}$), followed by the schist (0.0067 $m^{0.2}$) and then the mélange channels (0.0062 $m^{0.2}$). The three populations are not all drawn from the same distribution ($p < 0.001$). Non-KJf channels are significantly wider than channels in the mélange and the schist ($p < 0.001$ and $p = 0.006$, respectively), but there is no significant width difference between schist and mélange channel width ($p = 0.563$).

The differences in mean channel steepness between the three lithologies could have several causes. One could be the in situ erodibility, without accounting for potential boulder delivery, of the bedrock being incised. In particular, channels in the schist may be steeper than those in the mélange because schist is more erosion-resistant than the pervasively sheared, low-grade metasedimentary rocks of the mélange. Evidence from geotechnical tests suggests that the shear strength of the mélange increases with the proportion of schist boulders in the sample tested (Roadifer et al., 2009). This indicates that the

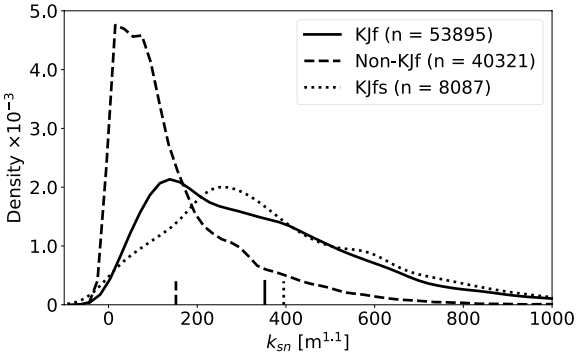

Figure 4. Density plots showing the distributions of channel steepness broken down by lithology. We separated the study area into the Franciscan mélange (mapped as KJf and KJfm, here referred to as KJf), the Franciscan schist (KJfs), and all other units (non-KJf). Apparent channel steepness values below zero are simply an artifact of the kernel density estimator; there are no steepness values below zero. Small vertical lines indicate the mean of each population. Kruskal-Wallis H-tests reveal that not all means are from the same distribution ($p < 0.001$); Dunn's posthoc tests using Holm corrections for multiple comparisons show that each of the three populations is statistically distinct from the others ($p < 0.001$ for all pairs).

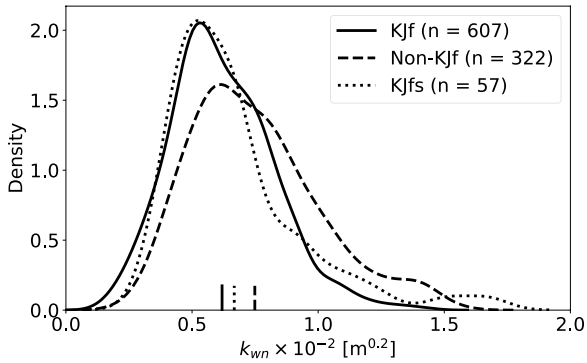

Figure 5. Density plots showing the distributions of channel width indices broken down by lithology. We separated the study area into the Franciscan mélange (mapped as KJf and KJfm, here referred to as KJf), the Franciscan schist (KJfs), and all other units (non-KJf). Small vertical lines indicate the mean of each population. Kruskal-Wallis H-tests suggest that not all means are from the same distribution ($p < 0.001$). Dunn's posthoc tests using Holm corrections for multiple comparisons show that non-KJf channels are significantly wider than mélange channels and schist channels ($p < 0.001$ and $p = 0.006$, respectively). Width differences between the mélange and schist channels are not statistically significant ($p = 0.563$).

schist boulders are more resistant than the matrix of the mélange. It is therefore probable that the erodibility of the schist, which lacks a highly sheared matrix, is lower than that of the mélange.

It is also possible that spatial variability in erosion rates caused by a tectonically driven wave of transient incision happens to cause higher erosion rates in the eastern portions of our study area, where the mélange and schist are most common, relative to the western area underlain by non-KJf units. If the current state of landscape transience leads to higher erosion rates in the mélange and schist, channels in those units may be steeper than channels in the non-KJf units even without lithologically controlled differences in channel response among the three units. Erodibility and erosion rate controls are not mutually exclusive; we discuss them further below.

Subcatchment Lithology and Channel Steepness

To investigate the potential relationship between lithology and channel steepness at the landscape scale, we used 344 sample subcatchments with drainage areas of between 10 km^2 and 50 km^2 (Figs. 1G and 1H). Figure 6 shows the mean channel steepness for each subcatchment as a function of the proportion of that subcatchment underlain by mélange (Fig. 6A), non-KJf (Fig. 6B), and schist (Fig. 6C). Catchments with greater proportions of mélange and schist tend to be steeper. Spearman rank correlation tests show significant ($p < 0.001$) positive correlations for both the mélange (Fig. 6A) and schist (Fig. 6C), with nearly identical effect sizes (ρ values) for the two units. Ninety-five percent confidence intervals (CIs) for the two correlation coefficients encompass only positive correlations (Figs. 6A and 6C). The proportion of a catchment underlain by non-KJf rocks must then be negatively correlated with channel steepness (Fig. 6B), as it is simply the remaining fraction of the catchment area. Figure 6 confirms that there exists a relationship between the lithological makeup of a subcatchment and that subcatchment's mean channel steepness. The proportions of mélange and schist, which must be (and are) negatively correlated with one another, exert similar effects on catchment-averaged steepness. A Spearman partial correlation analysis shows that the correlation between proportion of mélange and mean steepness, with the effects of schist removed, gives a correlation coefficient of $\rho = 0.49$ (95% CI: 0.40–0.57), while the same test for the schist (i.e., removing the effects of mélange) gives $\rho = 0.43$ (95% CI: 0.34–0.52). Both relationships are statistically significant ($p < 0.001$). We find that it is not simply the presence of mélange that is associated with steeper channels as found by Bennett et al. (2016), but the presence of mélange or schist (or equivalently, the absence of non-KJf units).

The Effect of Landslide Proximity on Channel Form

Figure 7 shows the basin-averaged distance to nearest hillslope failure for each subcatchment, a proxy for sediment supply to the channel by hillslope failures, plotted against

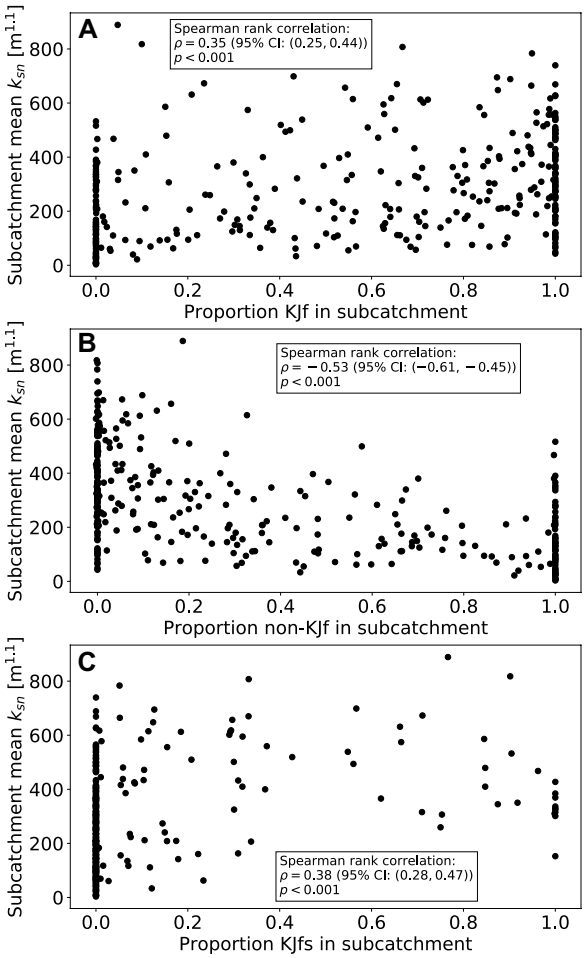

Figure 6. Relationship between the lithological makeup of a subcatchment and that subcatchment's mean channel steepness. Each data point represents one of the 344 subcatchments shown in Figures 1G and 1H. Panels show steepness as a function of the proportion of the subcatchment underlain by (A) mélange, (B) non-KJf, and (C) schist. Spearman rank correlation tests indicate that there are statistically significant relationships between lithology and catchment-averaged channel steepness. Partial correlation tests to separate the influence of the mélange and schist indicate that they have approximately the same effect on steepness.

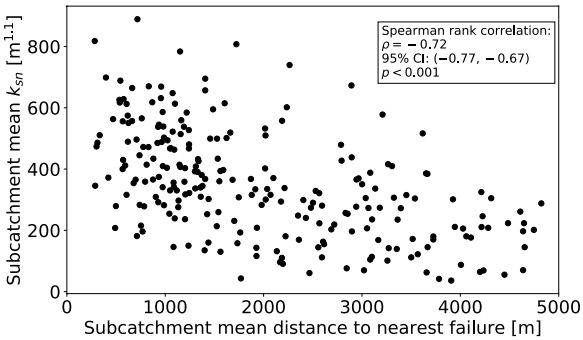

Figure 7. Relationship between subcatchment-averaged mean distance between each channel segment and its nearest hillslope failure and subcatchment-averaged mean channel steepness. Statistical relationships use all 344 subcatchments, but plot is zoomed in for clarity; only catchments with mean distance to nearest failure of less than 5 km are shown. There is a significant negative correlation between mean failure distance and mean channel steepness, and the 95% confidence interval encompasses only negative correlations. Partial correlation tests, conducted to isolate the effect of failure proximity from the influence of mélange occurrence in the subcatchments, show that proximity to failure is the stronger predictor of subcatchment-averaged channel steepness.

catchment-averaged channel steepness. Subcatchments with hillslope failures nearer to channels have higher mean steepness; we confirmed the significance of this relationship ($p < 0.001$) using the same statistical procedure as in Figure 6. The 95% confidence interval encompasses only negative correlations between mean distance to failure and mean channel steepness. We used a partial correlation analysis to test the relative effects of the proportion of each subcatchment underlain by mélange (Fig. 6A) and mean distance to the nearest hillslope failure (Fig. 7) on subcatchment-averaged channel steepness. When controlling for the proportion of mélange, mean distance to nearest hillslope failure is strongly, negatively correlated with mean channel steepness ($\rho = -0.51$, 95% CI: −0.58 to −0.43, $p < 0.001$). The relationship between proportion of mélange and mean steepness when controlling for mean distance to nearest failure is still statistically significant but much weaker ($\rho = 0.148$, 95% CI: 0.04–0.25, $p = 0.006$). Mean distance to nearest hillslope failure is the stronger predictor of channel steepness in the landscape as a whole, likely due to failures in all lithologies reflecting higher erosion rates.

In Figures 8A–8C, we present all channel steepness measurements as a function of distance to the nearest hillslope failure, separated by lithology. All three units show significant correlations ($p < 0.001$) between steepness and distance to failure, with 95% confidence intervals encompassing only negative correlations. We show in Figures 8D–8F the distributions of channel steepness index for each lithologic group, separated based on whether they are less than 100 m ("near") or greater than 100 m ("far") from the nearest hillslope failure. For all three lithologic groups, channels near hillslope failures are on average steeper than channels far from the nearest failure. In all three cases, we observe a statistically significant (as determined by Mann-Whitney U-tests), approximate doubling in mean channel steepness between channels far from failures and those near failures ($p < 0.001$). The size of the effect of failure proximity on channel steepness is approximately the same for all units (see Fig. 8 caption). The mélange channels increase on average from 335 m$^{1.1}$ to 614 m$^{1.1}$, the schist channels increase from 386 m$^{1.1}$ to 656 m$^{1.1}$, and the non-KJf channels increase from 149 m$^{1.1}$ to 359 m$^{1.1}$. Despite the relative paucity of earthflows in the schist, schist channels experience approximately the same proportional increase in steepness as mélange and non-mélange channels. While earthflows are more prevalent in the mélange, they do not seem to steepen channels more than hillslope failures in the other units do. The similar response to failure proximity in all lithologies suggests that erosion rate variations, by simultaneously driving the locations of steeper channels and failure-prone hillslopes, might outcompete lithology as an influence on the relationship between failure proximity and channel steepness.

Figure 9 shows the results of the same analysis for the channel width index data. While the mélange channels show significant ($p < 0.001$) narrowing with increased proximity to failures (Fig. 9A), non-KJf channels show significant ($p < 0.001$) widening with increased proximity (Fig. 9B). Schist channel widths are not significantly correlated ($p = 0.14$) with failure proximity (Fig. 9C). Only the mélange channel width values show a statistically significant ($p < 0.001$) difference between channels near (<100 m from) hillslope failures and those far (>100 m) from failures; mélange channels near failures are narrower than those far from failures (k_w of 0.0055 m$^{0.2}$ and 0.0064 m$^{0.2}$, respectively). Small sample sizes for channel width measurements within 100 m of hillslope failures in the non-KJf and schist make it difficult to test the effect of close failure proximity on width, but our data set does not indicate a significant effect in those units ($p = 0.11$ for non-KJf, $p = 0.25$ for schist). It is interesting but puzzling that the three units show such different width responses to hillslope failure proximity. Different rock strength properties and sediment grain size distributions may cause different width responses, or natural width variability may be too great to assess failure proximity controls within our data set.

Boulder Size Distributions and Concentrations

If boulder delivery by hillslope failures causes steepening in mélange channels relative to channels in the non-KJf units and the schist, we should observe greater concentrations of boulders per unit channel area (caused by more boulders, larger boulders, or both) at the toes of failures in mélange channels than at the toes of failures in non-KJf and schist channels. We present boulder mapping results from all three units in Figure 10. Box and whisker plots show the boulder size distributions (truncated at a minimum boulder long axis length of 2 m), and numbers beneath each box and whisker plot report the total number of boulders >2 m found. Labels indicate the type of failure as mapped by Bennett et al. (2016). There are more boulders, and larger boulders, in failure-adjacent mélange channels than in failure-adjacent non-KJf and schist channels. To eliminate the potentially biasing effects of measurement area, we calculated a dimensionless boulder concentration N_b (see methods) for each measurement site. The mean boulder concentration in channels at failure toes is over four times greater (0.19 versus 0.04) in mélange channels than in non-KJf channels. Schist channels have intermediate boulder concentrations (0.11).

Statistical analysis of boulder size distributions (a Kruskal-Wallis H-test, combined with Dunn's posthoc tests with Holm corrections for multiple comparisons) reveals that mélange channels host significantly larger boulders than both other units ($p < 0.001$ for both), but boulder size is not significantly different between the non-KJf and schist units ($p = 0.55$). The same tests on the boulder concentration data show that mélange channels have significantly greater boulder concentrations than non-KJf channels ($p = 0.005$), but that no other differences are significant ($p > 0.01$ for all others).

The presence of more large boulders and greater boulder concentrations in mélange channels could be one explanation for why mélange channels near hillslope failures are so much

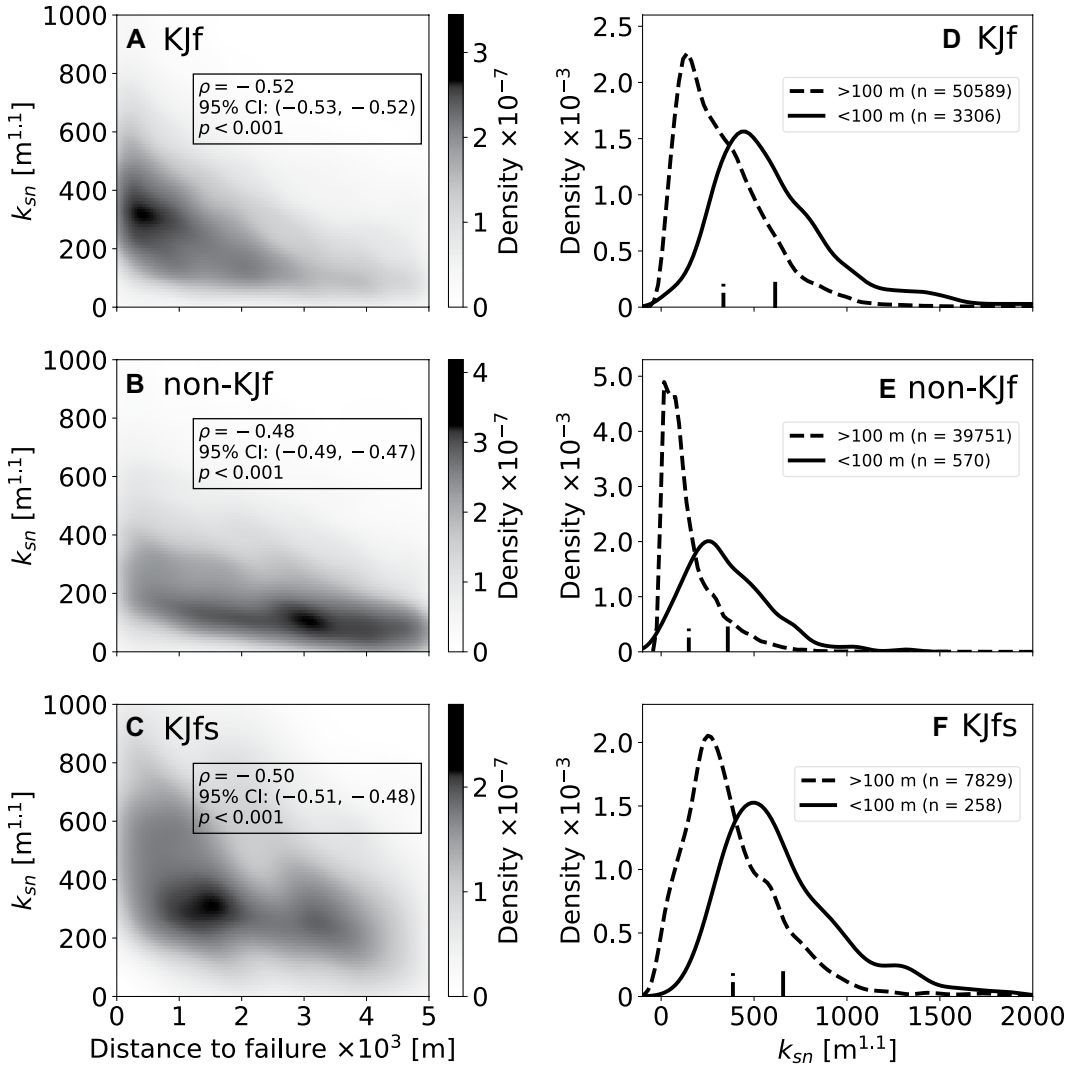

Figure 8. (A–C) Two-dimensional density plots showing the relationship between proximity to nearest hillslope failure and channel steepness index for each lithology. We used density plots because of the large number (order 10^4) of measurements in each unit. Statistical tests reported on the figure and in the text represent the entire data set, but we display only channel segments with failure proximity under 5 km for clarity. All lithologies show statistically significant, positive correlations between failure proximity (or equivalently, negative correlations with failure distance) and channel steepness. (D–F) Density plots showing the distributions for each lithology of channels near (<100 m) and far (>100 m) from the nearest mapped hillslope failure (solid lines and dashed lines, respectively). Small vertical lines indicate the mean of each population. In all three units, reaches near hillslope failures are steeper on average than reaches far from hillslope failures. The differences between channels near and far from hillslope failures are statistically significant, as determined by Mann-Whitney U-tests, in all three lithological groups ($p < 0.001$). Effect sizes given by the common language effect are approximately the same for the three units (0.77, 0.81, and 0.77 for the mélange, non-KJf, and schist, respectively). Mean channel steepness approximately doubles between the two populations in each lithology. In the KJf and KJfs units, steepness in channels both near and far from failures is approximately double that found in the non-KJf units.

steeper than near-failure non-KJf channels. However, it is also clear that boulder prevalence cannot be the only control on channel steepness in this landscape, as the unit with the steepest channels (the schist) does not have the greatest boulder sizes and concentrations. Below we use a numerical model to investigate the possible steepening that could be caused in the mélange by the boulder sizes and concentrations we observe. We also discuss other potential steepening mechanisms.

Numerical Modeling of the Influence of Boulders on Channel Steepness

Our numerical model uses established theory (Shobe et al., 2016, 2018; Glade et al., 2019) for how boulders inhibit erosion by armoring the channel bed and increasing hydraulic drag. We parameterized the model by using the mean values for boulder size (4 m) and channel area mapped (30,208 m^2) obtained from our mapping of boulders in mélange channels. We then varied the number of boulders to progressively increase the dimensionless boulder concentration N_b and show how N_b might influence channel slope relative to the no-boulders case (Fig. 11). Because the hydraulic effects of boulders depend on water discharge, we show curves representing two discharge scenarios at widely differing drainage areas to get a sense of the range of possible outcomes in our study region. We used the mean discharge per unit channel width (q) for the past 10 years from two gauges in our study area: the U.S. Geological Survey gauge at Leggett, California (gauge #11475800), which has a drainage area of 642 km^2 and a decade-averaged discharge per unit width of $q = 0.47$ m^2/s, and the Scotia, California, gauge (gauge #11477000), which drains 8063 km^2 and has a decade-averaged discharge per unit width of $q = 1.27$ m^2/s.

In Figure 11 we show the predicted increase in slope relative to the no-boulders case (S_b/S_i) as dimensionless boulder concentration N_b increases (black lines). We also highlight the N_b values we observed in the mélange channels from our boulder mapping (gray shaded region). The curve calculated with the higher specific discharge predicts greater steepening because increased flow depth results in greater drag stress due to boulders in the channel, which are not fully submerged at these discharges. Our calculations show that channel slopes could increase several-fold relative to the no-boulders case given the boulder sizes and concentrations we found in the mélange channels if two key

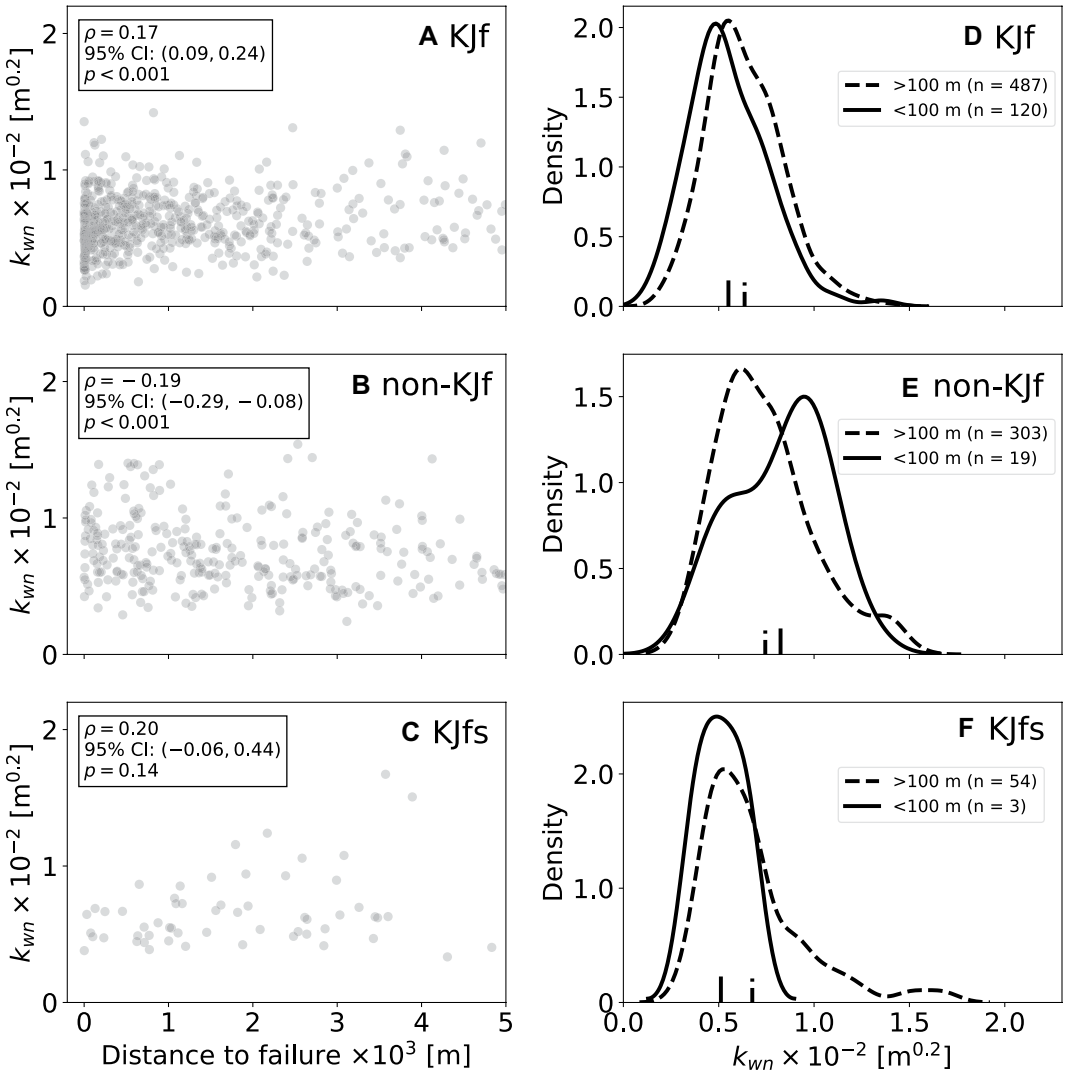

Figure 9. (A–C) Scatter plots showing the relationship between proximity to nearest hillslope failure and channel width index for each lithology. Statistical tests reported on the figure and in the text represent the entire data set, but we display only channel segments with failure proximity under 5 km for clarity. KJf channels show a statistically significant decrease in width with increasing failure proximity (decreasing failure distance), while non-KJf channels show a significant increase in width with increasing failure proximity. Channels in the KJfs do not show a significant relationship between failure proximity and width. (D–F) Density plots showing the distributions for each lithology of channels near (<100 m) and far (>100 m) from the nearest hillslope failure (solid lines and dashed lines, respectively). Small vertical lines indicate the mean of each population. Mann-Whitney U-tests show that only the mélange channels exhibit a statistically significant ($p < 0.001$) difference in width index between measurements near hillslope failures and measurements far from hillslope failures, though it is important to note that subdivision of the data has resulted in small sample sizes for failure-adjacent channels in the non-KJf ($p = 0.11$) and the schist ($p = 0.25$).

model assumptions are met: (1) boulders do not become mobile and (2) channel width does not substantially change as slope increases due to the presence of boulders. The validity of this latter assumption may vary between lithologies (Fig. 9). Given that the observed average boulder concentration value for mapped mélange channels was $N_b = 0.19$, our model suggests that boulder delivery alone could result in mélange channels that are two-fold to three-fold steeper than non-KJf channels experiencing little boulder delivery. Modeling results show maximum expected channel steepening; there exists for any discharge a slope above which boulders of a given size would be mobile where the model would no longer apply. Further, inconsistent boulder supply over the timescale of channel slope adjustment could lead to processes such as epigenetic gorge formation (see discussion by Finnegan et al., 2019) that are not captured by our model.

Erosion Rate, Rock Erodibility, and Boulder Delivery Controls on Channel Steepness

Our analysis reveals that the highest boulder concentrations occur in mélange channels with moderate concentrations in the schist and low concentrations in non-KJf channels. Steady-state modeling suggests that observed boulder prevalence in the mélange could explain observed channel steepness patterns. Boulder delivery, however, is only one of three possible controls on channel steepness in our study area; the others are spatial variability in erosion rates due to transient adjustment of our study area to forcing by Mendocino triple junction tectonics, and differences in in situ rock erodibility between lithologies.

The greatest relative increase in channel steepness with failure proximity occurs in the non-KJf channels. This result could be interpreted as evidence that non-KJf channels experience the most steepening due to hillslope failure proximity, and therefore that proximity to hillslope failures does not affect mélange channel steepness any more than it does non-KJf channel steepness. In this interpretation, the increased overall and subcatchment-averaged channel steepness in areas underlain by the mélange and schist would have to be caused by lower rock erodibility in those two units or spatially variable erosion rates in which high erosion rates happen to coincide with areas underlain by mélange and schist.

However, the relationship between erosion rate and channel steepness in this landscape, as

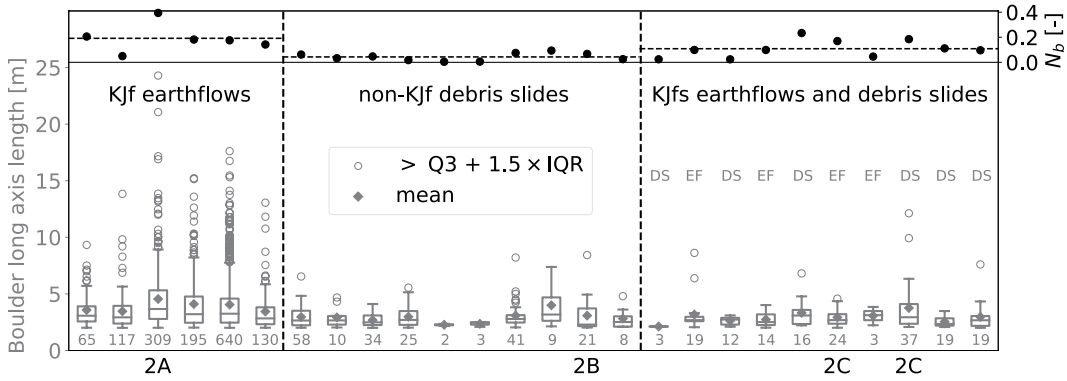

Figure 10. Results of in-channel boulder mapping. We only mapped boulders with a long axis of >2 m, imposed by the resolution of the satellite imagery. Box and whisker plots show the sizes of boulders mapped, and numbers beneath each plot give the total number of boulders >2 m found. Measurements rendered as individual points are those that exceed the third quartile by more than 1.5 times the inter-quartile range. Labels on the schist portion of the plot indicate whether the failure was mapped by Bennett et al. (2016) as an earthflow or a debris slide. Labels below the *x*-axis show the locations of the images in Figure 2. The upper plot gives the dimensionless boulder concentration (N_b; Equation 4), a measure of boulder size and frequency that is independent of the area surveyed. The mean value of N_b is nearly five times higher for hillslope failures in the mélange than it is for failures in the non-KJf. The schist exhibits intermediate behavior, with boulder concentrations over twice as high as non-KJf channels but substantially lower than mélange channels. Kruskal-Wallis H-tests show that boulder sizes in mélange channels are significantly different ($p < 0.001$) from those in both other units, but boulder sizes in non-KJf channels are not significantly different from those in schist channels ($p = 0.55$). Boulder concentrations in the mélange are significantly greater than those in non-KJf channels ($p = 0.005$) but not greater than than those in the schist ($p = 0.19$). Boulder concentrations are not statistically different between the schist and the non-KJf ($p = 0.07$). Locations of mapping sites are available in the Data Repository. Images used for mapping are available in a permanent repository (Shobe et al., 2020).

in many landscapes (e.g., Snyder et al., 2003a, 2003b; Tucker, 2004; Lague et al., 2005; DiBiase and Whipple, 2011; Scherler et al., 2017), is nonlinear. The erosion rate—channel steepness relationship derived for the Mendocino triple junction region by Bennett et al. (2016) (Fig. 3) shows that a given increase in erosion rate results in less steepening at higher erosion rates than it would at lower erosion rates. If erosion rate variations alone set channel steepness, the increase in erosion rate required to explain the near-doubling in steepness with failure proximity in mélange and schist channels would be much greater than the increase in erosion rate required to explain the more than doubled steepness observed in the non-KJf channels. This does not rule out erosion rate variations as an influence on channel steepness, but it does suggest a role for an additional driver of steepening in the mélange and schist besides erosion rate alone. Possible candidates include reduced rock erodibility and the delivery of large boulders.

Adding further complexity is the possibility that the migration of steepened channel reaches (knickpoints) created by rapid rock uplift through the boulder-yielding mélange may be slowed by boulder delivery to the channel, as suggested by Bennett et al. (2016). This process could result in steep reaches that migrate quickly through boulder-poor channels but persist longer in boulder-rich lithologies. However, the presence of "relict" topography in both the non-KJf (Foster and Kelsey, 2012; Willenbring et al., 2013) and the mélange and schist (Roering et al., 2015; Bennett et al., 2016) suggests that the transient signal of rock uplift has not propagated through the entire river network. How much rock uplift rates vary from east to west is an important question for further study and could be an alternate explanation for some of the observed steepening.

Contrasts in erodibility among the different bedrock lithologies in our study area may also influence channel steepness. It is possible that the mélange may be more erosion resistant, even in the absence of boulder delivery, than the non-KJf units (and nearly as erosion resistant as the schist). Even without boulder delivery from earthflows, resistant boulders can still be exhumed from the channel bed and banks. This difference in erodibility between the mélange and the non-KJf units could explain increased steepness in mélange channels relative to non-KJf channels as well as similar steepness values between the mélange and schist. Boulders in this

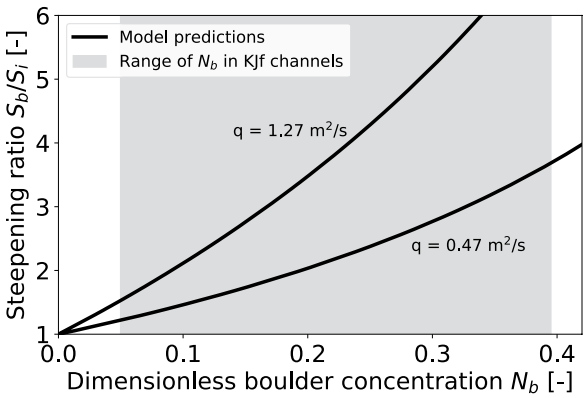

Figure 11. Numerical model predictions for channel steepening due to the presence of boulders as a function of dimensionless boulder concentration N_b (Equation 4). The steepening ratio S_b/S_i is the slope of a boulder-influenced modeled channel reach S_b normalized by the slope of a modeled reach experiencing the same erosion rate without any boulders S_i. The numerical model is parameterized with the average boulder size (4 m) found in mélange channels. The black lines show model predictions for two hydrologic scenarios: a discharge per unit width of $q = 1.27$ m²/s, the 10-year mean at the U.S. Geological Survey (USGS) gauge at Scotia near the mouth of the Eel River (drainage area of 8063 km²), and a discharge per unit width of $q = 0.47$ m²/s, the 10-year mean at the USGS gauge at Leggett, which is much farther upstream on the South Fork Eel River (drainage area of 642 km²). The gray zone shows the range of N_b values found in mélange channels (Fig. 10). The model suggests that the boulder concentrations mapped in the Franciscan mélange (average $N_b = 0.19$) could contribute to two-fold to three-fold channel steepening relative to non-KJf channels (average $N_b = 0.04$), assuming that the channel does not achieve the slope necessary to mobilize 4 m boulders.

case would still play a role in setting landscape response to tectonic perturbations, but the role of earthflows as agents of boulder delivery may be unimportant if sufficient quantities of boulders can be exhumed to the surface by river erosion alone. The recent analysis of Finnegan et al. (2019), however, suggests that this is unlikely, at least in smaller channels where the locations of valleys blocked by boulder deposits correspond to the locations of mapped earthflows.

We suggest that a more likely possibility is that channels in the Franciscan schist are eroding more resistant bedrock than mélange channels and many non-KJf channels. The geologic map unit descriptions (Jennings, 1977), geotechnical tests (Roadifer et al., 2009), and the prevalence of earthflows in the mélange give reason to believe that the schist is mechanically stronger, and therefore more resistant to erosion, than the pervasively sheared graywacke and mudstone that make up the matrix of the mélange. If true, this would help explain why schist channels are steeper than mélange channels (Fig. 4) even though schist channels have lower boulder concentrations and the co-location of the two units in space (Fig. 1C) makes it unlikely that they are experiencing very different erosion rates. We tentatively suggest the possibility that the schist is less erodible than the mélange and that increased boulder concentrations in the mélange reduce what would otherwise be greater steepness differences between the two. Our findings that mélange channels contain larger boulders and higher boulder concentrations than the schist (Fig. 10), and that observed boulder concentrations in the mélange could be enough to drive substantial channel steepening (Fig. 11), support the feasibility of this mechanism. However, it is impossible from the field data alone to dismiss the null hypothesis that erodibility and erosion rates are similar between the mélange and schist but different in the non-KJf units, and that boulder delivery does not have a first-order effect on channel form.

The work of Finnegan et al. (2019) raises a final important point about river response to boulder delivery in this region. Their finding that smaller channels exhibit knickpoint lips composed of jammed boulders means that some of the channel steepness variations we measured are due to surficial sediment dynamics rather than the slope of the underlying bedrock surface. Except by visual inspection, it would not be possible to distinguish these two effects. However, the valley blocking mechanism proposed by Finnegan et al. (2019), if boulder deposits were long-lived, would ultimately result in the type of adjustments to bedrock channel gradient treated by our model. We also note that all but one of our mélange boulder mapping sites were in large channels that did not show evidence for boulder jamming; our modeling suggests that the boulder concentrations observed in those larger channels are large enough to cause adjustment of the channel bedrock surface if boulder delivery persists through time. Boulder jamming, which we do not model, would enhance this effect. Jamming provides a compelling explanation for boulder-induced steepening in low-order channels; long-term steepening of the channel bed due to high concentrations of erosion-inhibiting boulders may have a similar but more subtle effect in larger channels.

Implications for Landscape Response to Tectonics

Though we cannot fully separate the effects of erosion rate and erodibility variations in our morphometric analysis, our boulder mapping and numerical modeling results provide some support for the idea that boulder delivery to channels in the mélange—and to a lesser extent the schist—may slow landscape adjustment to tectonic forcing at the Mendocino triple junction and aid the preservation of high-elevation, low-relief topography. Rock-type-dependent boulder delivery is a mechanism by which the lithological heterogeneity of tectonically active landscapes could control topographic response to transient tectonic perturbations.

Boulder-mantled river channels are a manifestation of a set of channel-hillslope feedbacks that can cause erosional responses to tectonics to be highly nonuniform in space and unsteady in time (Shobe et al., 2016; Glade et al., 2019). While a unit with lower in situ rock erodibility can be expected to slow the transmission of erosional signals through the channel network, the signal propagation rate is predictable given knowledge of the tectonic forcing and rock erodibility. Boulder delivery feedbacks are more complex because of the dynamic interactions among river erosion processes that set hillslope gradient, hillslope processes that control boulder delivery to the channel, and the resulting influence of hillslope-derived boulders on river erosion rates. Landscape resistance to river erosion—at least in lithologies that produce boulders—is not simply an in situ property but is a state variable driven by interactions between river erosion and hillslope evolution processes. These interactions, modulated by the unique sediment transport mechanisms and grain size distributions imposed by each rock type, have the potential to cause a great diversity in patterns and timescales of landscape adjustment to tectonic forcing.

CONCLUSIONS

Understanding landscape evolution in the presence of transient tectonic signals is critical to constraining Earth's sediment mass balance, but the role of rock properties—including sediment grain size—is not well understood. Our goal was to investigate a possible lithologic control on river and landscape response to rock uplift and the preservation of high-elevation, low-relief topography in the Mendocino triple junction region: preferential boulder delivery to channels in the Franciscan mélange relative to other rock units. We synthesized observations of river channel morphology, bedrock lithology, hillslope failure proximity, and boulder size, frequency, and concentration. We also introduced a simple, steady-state numerical model for channel slope adjustment to the presence of boulders.

Our analysis of landscape morphology shows that channels in the mélange and schist are steeper, both on average and near hillslope failures, than Coastal Belt channels. Because we cannot rule out the effects of variable rock erodibility and spatially varying erosion rates on observed channel steepness patterns, it is not possible to evaluate with certainty the idea that boulder delivery to mélange channels is the primary cause of channel steepening—and the preservation of relict high topography—in this landscape. The fact that the steepest channels in the study site (failure-adjacent channels in the schist) do not have the highest boulder concentrations means that boulder delivery cannot be the only factor involved. However, our boulder mapping shows that boulder delivery is indeed more common in the mélange. Mélange channels host significantly larger boulders and higher boulder concentrations than other units; this supports Bennett et al.'s (2016) hypothesis that boulder delivery occurs preferentially in mélange channels.

Numerical modeling parameterized with field data suggests that the boulder concentrations we observe could lead to two-fold to three-fold steepening due to boulder delivery in the mélange. We therefore suggest that though the landscape-scale signatures of boulder delivery are difficult to isolate, enough lithology-dependent boulder delivery occurs in the Mendocino triple junction region to cause differences in landscape adjustment between lithologies. More broadly, our results illuminate the ways in which channel-hillslope sediment delivery feedbacks may influence transient landscape response to tectonics (Egholm et al., 2013; Bennett et al., 2016; Shobe et al., 2016; Sklar et al., 2017; DiBiase et al., 2018; Glade et al., 2019). Untangling the external and internal controls over the response of Earth's surface to transient tectonic perturbations is an ongoing challenge. Sediment grain size variations driven by lithologic variability have the potential to govern landscape response, set the lifespan of high

topography, and thereby imprint the effects of rock type on landscape form and evolution over geologic time.

ACKNOWLEDGMENTS

The data and scripts used to generate Figures 3–11, as well as the original and annotated photos used for boulder mapping, are permanently archived in a Figshare repository (https://doi.org/10.6084/m9.figshare.11956836.v1). We thank National Science Foundation EAR-1331828 (the Boulder Creek Critical Zone Observatory) for funding. C.M. Shobe was supported by a National Defense Science and Engineering graduate fellowship, a University of Colorado Chancellor's fellowship, a Geological Society of America graduate student grant, and a University of Colorado Beverly Sears grant. Thanks to Bob Anderson, Jason Kean, Peter Molnar, and Kelin Whipple for reading an early draft, and to Katy Barnhart, Noah Finnegan, Rachel Glade, Kim Huppert, Aaron Hurst, Kelly Kochanski, Simon Kübler, and Matt Rossi for helpful discussions. Reviews by Dan Scott, one anonymous reviewer, Associate Editor Karl Wegmann, and Editor Wenjiao Xiao greatly improved the paper.

REFERENCES CITED

Allen, G.H., Barnes, J.B., Pavelsky, T.M., and Kirby, E., 2013, Lithologic and tectonic controls on bedrock channel form at the northwest Himalayan front: Journal of Geophysical Research: Earth Surface, v. 118, p. 1806–1825, https://doi.org/10.1002/jgrf.20113.

Balco, G., Finnegan, N., Gendaszek, A., Stone, J.O.H., and Thompson, N., 2013, Erosional response to northward-propagating crustal thickening in the coastal ranges of the U.S. Pacific Northwest: American Journal of Science, v. 313, p. 790–806, https://doi.org/10.2475/11.2013.01.

Bennett, G.L., Miller, S.R., Roering, J.J., and Schmidt, D.A., 2016, Landslides, threshold slopes, and the survival of relict terrain in the wake of the Mendocino Triple Junction: Geology, v. 44, p. 363–366, https://doi.org/10.1130/G37530.1.

Braun, D.D., 1983, Lithologic control of bedrock meander dimensions in the Appalachian Valley and Ridge province: Earth Surface Processes and Landforms, v. 8, p. 223–237, https://doi.org/10.1002/esp.3290080305.

Brown, W.M., and Ritter, J.R., 1971, Sediment transport and turbidity in the Eel River basin, California: U.S. Geological Survey Water-Supply Paper 1986, 70 p.

Bursztyn, N., Pedersen, J.L., Tressler, C., Mackley, R.D., and Mitchell, K.J., 2015, Rock strength along a fluvial transect of the Colorado Plateau—Quantifying a fundamental control on geomorphology: Earth and Planetary Science Letters, v. 429, p. 90–100, https://doi.org/10.1016/j.epsl.2015.07.042.

Chatanantavet, P., and Parker, G., 2009, Physically based modeling of bedrock incision by abrasion, plucking, and macroabrasion: Journal of Geophysical Research: Earth Surface, v. 114, F04018, https://doi.org/10.1029/2008JF001044.

Clubb, F.J., Mudd, S.M., Hurst, M.D., and Grieve, S.W.D., 2020, Differences in channel and hillslope geometry record a migrating uplift wave at the Mendocino triple junction, California, USA: Geology, v. 48, p. 184–188, https://doi.org/10.1130/G46939.1.

Cook, K.L., Andermann, C., Gimbert, F., Adhikari, B.R., and Hovius, N., 2018, Glacial lake outburst floods as drivers of fluvial erosion in the Himalaya: Science, v. 362, p. 53–57, https://doi.org/10.1126/science.aat4981.

Deal, E., Braun, J., and Botter, G., 2018, Understanding the role of rainfall and hydrology in determining fluvial erosion efficiency: Journal of Geophysical Research: Earth Surface, v. 123, p. 744–778, https://doi.org/10.1002/2017JF004393.

DiBiase, R.A., and Whipple, K.X., 2011, The influence of erosion thresholds and runoff variability on the relationships among topography, climate, and erosion rate: Journal of Geophysical Research: Earth Surface, v. 116, F04036, https://doi.org/10.1029/2011JF002095.

DiBiase, R.A., Rossi, M.W., and Neely, A.B., 2018, Fracture density and grain size controls on the relief structure of bedrock landscapes: Geology, v. 46, p. 399–402, https://doi.org/10.1130/G40006.1.

Ding, X., Salles, T., Flament, N., Mallard, C., and Rey, P.F., 2019, Drainage and sedimentary responses to dynamic topography: Geophysical Research Letters, v. 46, https://doi.org/10.1029/2019GL084400.

Duvall, A., Kirby, E., and Burbank, D., 2004, Tectonic and lithologic controls on bedrock channel profiles and processes in coastal California: Journal of Geophysical Research: Earth Surface, v. 109, p. F03002, https://doi.org/10.1029/2003JF000086.

Egholm, D.L., Knudsen, M.F., and Sandiford, M., 2013, Lifespan of mountain ranges scaled by feedbacks between land sliding and erosion by rivers: Nature, v. 498, p. 475–478, https://doi.org/10.1038/nature12218.

Ferguson, R., 2007, Flow resistance equations for gravel- and boulder-bed streams: Water Resources Research, v. 43, W05427, https://doi.org/10.1029/2006WR005422.

Ferrier, K.L., and Kirchner, J.W., 2008, Effects of physical erosion on chemical denudation rates: A numerical modeling study of soil-mantled hillslopes: Earth and Planetary Science Letters, v. 272, p. 591–599, https://doi.org/10.1016/j.epsl.2008.05.024.

Finnegan, N.J., Klier, R.A., Johnstone, S., Pfeiffer, A.M., and Johnson, K., 2017, Field evidence for the control of grain size and sediment supply on steady-state bedrock river channel slopes in a tectonically active setting: Earth Surface Processes and Landforms, v. 42, p. 2338–2349, https://doi.org/10.1002/esp.4187.

Finnegan, N.J., Broudy, K.N., Nereson, A.L., Roering, J.J., Handwerger, A.L., and Bennett, G., 2019, River channel width controls blocking by slow-moving landslides in California's Franciscan mélange: Earth Surface Dynamics, v. 7, p. 879–894, https://doi.org/10.5194/esurf-7-879-2019.

Forte, A.M., Whipple, K.X., Bookhagen, B., and Rossi, M.W., 2016, Decoupling of modern shortening rates, climate, and topography in the Caucasus: Earth and Planetary Science Letters, v. 449, p. 282–294, https://doi.org/10.1016/j.epsl.2016.06.013.

Foster, M.A., and Kelsey, H.M., 2012, Knickpoint and knickzone formation and propagation, South Fork Eel River, northern California: Geosphere, v. 8, p. 403–416, https://doi.org/10.1130/GES00700.1.

Furlong, K.P., and Govers, R., 1999, Ephemeral crustal thickening at a triple junction: The Mendocino crustal conveyor: Geology, v. 27, p. 127–130, https://doi.org/10.1130/0091-7613(1999)027<0127:ECTAAT>2.3.CO;2.

Gasparini, N.M., Whipple, K.X., and Bras, R.L., 2007, Predictions of steady state and transient landscape morphology using sediment-flux-dependent river incision models: Journal of Geophysical Research: Earth Surface, v. 112, F03S09, https://doi.org/10.1029/2006JF000567.

Gilbert, G.K., 1877, Report on the Geology of the Henry Mountains: Washington, D.C., U.S. Geological Survey of the Rocky Mountain Region, 160 p.

Glade, R.C., Shobe, C.M., Anderson, R.S., and Tucker, G.E., 2019, Canyon shape and erosion dynamics governed by channel-hillslope feedbacks: Geology, v. 47, no. 7, p. 650–654, https://doi.org/10.1130/G46219.1.

GRASS Development Team, 2018, Geographic Resources Analysis Support System (GRASS) Software, Version 7.4: Open Source Geospatial Foundation, Electronic document, http://grass.osgeo.org.

Hack, J.T., 1965, Geomorphology of the Shenandoah Valley, Virginia and West Virginia, and Origin of the Residual Ore Deposits: U.S. Geological Survey Professional Paper 484, 88 p., https://doi.org/10.3133/pp484.

Handwerger, A.L., Roering, J.J., Schmidt, D.A., and Rempel, A.W., 2015, Kinematics of earthflows in the Northern California Coast Ranges using satellite interferometry: Geomorphology, v. 246, p. 321–333, https://doi.org/10.1016/j.geomorph.2015.06.003.

Hilley, G.E., Porder, S., Aron, F., Baden, C.W., Johnstone, S.A., Liu, F., Sare, R., Steelquist, A., and Young, H.H., 2019, Earth's topographic relief potentially limited by an upper bound on channel steepness: Nature Geoscience, v. 12, p. 828–832, https://doi.org/10.1038/s41561-019-0442-3.

Hobley, D.E.J., Sinclair, H.D., Mudd, S.M., and Cowie, P.A., 2011, Field calibration of sediment flux dependent river incision: Journal of Geophysical Research: Earth Surface, v. 116, F04017, https://doi.org/10.1029/2010JF001935.

Howard, A.D., 1994, A detachment-limited model of drainage basin evolution: Water Resources Research, v. 30, no. 7, p. 2261–2285, https://doi.org/10.1029/94WR00757.

Howard, A., and Dolan, R., 1981, Geomorphology of the Colorado River in the Grand Canyon: The Journal of Geology, v. 89, p. 269–298, https://doi.org/10.1086/628592.

Hungr, O., Leroueil, S., and Picarelli, L., 2014, The Varnes classification of landslide types, an update: Landslides, v. 11, p. 167–194, https://doi.org/10.1007/s10346-013-0436-y.

Iverson, R.M., and Major, J.J., 1987, Rainfall, ground-water flow, and seasonal movement at Minor Creek landslide, northwestern California: Physical interpretation of empirical relations: Geological Society of America Bulletin, v. 99, p. 579–594, https://doi.org/10.1130/0016-7606(1987)99<579:RGFASM>2.0.CO;2.

Jennings, C.W., 1977, Geologic Map of California, Geologic Data Map Series Map 2, scale 1:750000. Sacramento, California.

Johnson, J.P.L., Whipple, K.X., Sklar, L.S., and Hanks, T.C., 2009, Transport slopes, sediment cover, and bedrock channel incision in the Henry Mountains, Utah: Journal of Geophysical Research, v. 114, p. F02014, https://doi.org/10.1029/2007JF000862.

Johnson, K.N., and Finnegan, N.J., 2015, A lithologic control on active meandering in bedrock channels: Geological Society of America Bulletin, v. 127, p. 1766–1776, https://doi.org/10.1130/B31184.1.

Kean, J.W., and Smith, J.D., 2004, Flow and boundary shear stress in channels with woody bank vegetation, *in* Bennett, S.J., and Simon, A., eds., Riparian Vegetation and Fluvial Geomorphology: Washington, D.C., American Geophysical Union, Water Science and Application Series, p. 237–252, https://doi.org/10.1029/008WSA17.

Kean, J.W., and Smith, J.D., 2010, Calculation of stage-discharge relations for gravel bedded channels: Journal of Geophysical Research: Earth Surface, v. 115, F03020, https://doi.org/10.1029/2009JF001398.

Keefer, D.K., and Johnson, A.M., 1983, Earth Flows: Morphology, Mobilization, and Movement: U.S. Geological Survey Professional Paper 1264, https://doi.org/10.3133/pp1264.

Kelsey, H.M., 1978, Earthflows in Franciscan mélange, Van Duzen River basin, California: Geology, v. 6, p. 361–364, https://doi.org/10.1130/0091-7613(1978)6<361:EIFMVD>2.0.CO;2.

Kelsey, H.M., 1980, A sediment budget and an analysis of geomorphic process in the Van Duzen River basin, north coastal California, 1941–1975: Geological Society of America Bulletin, v. 91, p. 1119–1216, https://doi.org/10.1130/GSAB-P2-91-1119.

Lague, D., 2010, Reduction of long-term bedrock incision efficiency by short-term alluvial cover intermittency: Journal of Geophysical Research: Earth Surface, v. 115, F02011, https://doi.org/10.1029/2008JF001210.

Lague, D., 2014, The stream power river incision model: Evidence, theory, and beyond: Earth Surface Processes and Landforms, v. 39, p. 38–61, https://doi.org/10.1002/esp.3462.

Lague, D., Hovius, N., and Davy, P., 2005, Discharge, discharge variability, and the bedrock channel profile: Journal of Geophysical Research: Earth Surface, v. 110, F04006, https://doi.org/10.1029/2004JF000259.

Lock, J., Kelsey, H., Furlong, K., and Woolace, A., 2006, Late Neogene and Quaternary landscape evolution of the northern California Coast Ranges: Evidence for Mendocino triple junction tectonics: Geological Society of America Bulletin, v. 118, p. 1232–1246, https://doi.org/10.1130/B25885.1.

Mackey, B.H., and Roering, J.J., 2011, Sediment yield, spatial characteristics, and the long-term evolution of active earthflows determined from airborne LiDAR

and historical aerial photographs, Eel River, California: Geological Society of America Bulletin, v. 123, p. 1560–1576, https://doi.org/10.1130/B30306.1.

Marshall, J.A., and Roering, J.J., 2014, Diagenetic variation in the Oregon Coast Range: Implications for rock strength, soil production, hillslope form, and landscape evolution: Journal of Geophysical Research: Earth Surface, v. 119, p. 1395–1417, https://doi.org/10.1002/2013JF003004.

Mclaughlin, R.J., Ellen, S.D., Blake, J.M.C., Jayko, A.S., Irwin, W.P., Aalto, K.R., Carver, G.A., and Clarke, S.H., 2000, Geology of the Cape Mendocino, Eureka, Garberville, and southwestern part of the Hayfork 30×60 minute quadrangles and adjacent offshore area, Northern California: U.S. Geological Survey Miscellaneous Field Studies Map MF-2336, scale 1:100,000, 6 sheets.

Merritts, D.J., 1996, The Mendocino triple junction: Active faults, episodic coastal emergence, and rapid uplift: Journal of Geophysical Research: Solid Earth, v. 101, p. 6051–6070, https://doi.org/10.1029/95JB01816.

Merritts, D.J., and Bull, W.B., 1989, Interpreting Quaternary uplift rates at the Mendocino triple junction, northern California, from uplifted marine terraces: Geology, v. 17, p. 1020–1024, https://doi.org/10.1130/0091-7613(1989)017<1020:IQURAT>2.3.CO;2.

Merritts, D.J., and Vincent, K.R., 1989, Geomorphic response of coastal streams to low, intermediate, and high rates of uplift, Mendocino triple junction region, northern California: Geological Society of America Bulletin, v. 101, p. 1373–1388, https://doi.org/10.1130/0016-7606(1989)101<1373:GROCST>2.3.CO;2.

Molnar, P., 2001, Climate change, flooding in arid environments, and erosion rates: Geology, v. 29, p. 1071–1074, https://doi.org/10.1130/0091-7613(2001)029<1071:CCFIAE>2.0.CO;2.

Molnar, P., Anderson, R.S., Kier, G., and Rose, J., 2006, Relationships among probability distributions of stream discharges in floods, climate, bed load transport, and river incision: Journal of Geophysical Research: Earth Surface, v. 111, F02001, https://doi.org/10.1029/2005JF000310.

Moon, S., Merritts, D.J., Snyder, N.P., Bierman, P., Sanquini, A., Fosdick, J.C., and Hilley, G.E., 2018, Erosion of coastal drainages in the Mendocino Triple Junction region (MTJ), northern California: Earth and Planetary Science Letters, v. 502, p. 156–165, https://doi.org/10.1016/j.epsl.2018.09.006.

Murphy, B.P., Johnson, J.P.L., Gasparini, N.M., and Sklar, L.S., 2016, Chemical weathering as a mechanism for the climatic control of bedrock river incision: Nature, v. 532, p. 223–227, https://doi.org/10.1038/nature17449.

Nereson, A.L., and Finnegan, N.J., 2019, Drivers of earthflow motion revealed by an 80 yr record of displacement from Oak Ridge earthflow, Diablo Range, California, USA: Geological Society of America Bulletin, v. 131, p. 389–402, https://doi.org/10.1130/B32020.1.

Rasband, W., 2019, ImageJ image analysis software: Bethesda, Maryland, U.S. National Institutes of Health.

Roadifer, J.W., Forrest, M.P., and Lindquist, E.S., 2009, Evaluation of shear strength of mélange foundation at Calaveras Dam, *in* Proceedings of the 29th U.S. Society for Dams Annual Meeting and Conference, "Managing Our Water Retention Systems," Nashville, Tennessee.

Roering, J.J., Mackey, B.H., Handwerger, A.L., Booth, A.M., Schmidt, D.A., Bennett, G.L., and Cerovski-Darriau, C., 2015, Beyond the angle of repose: A review and synthesis of landslide processes in response to rapid uplift, Eel River, Northern California: Geomorphology, v. 236, p. 109–131, https://doi.org/10.1016/j.geomorph.2015.02.013.

Scherler, D., DiBiase, R.A., Fisher, G.B., and Avouac, J.-P., 2017, Testing monsoonal controls on bedrock river incision in the Himalaya and Eastern Tibet with a stochastic-threshold stream power model: Journal of Geophysical Research: Earth Surface, v. 122, p. 1389–1429, https://doi.org/10.1002/2016JF004011.

Schwanghart, W., and Scherler, D., 2014, Short communication: TopoToolbox 2- MATLAB-based software for topographic analysis and modeling in Earth surface sciences: Earth Surface Dynamics, v. 2, p. 1–7, https://doi.org/10.5194/esurf-2-1-2014.

Scott, D.N., and Wohl, E.E., 2019, Bedrock fracture influences on geomorphic process and form across process domains and scales: Earth Surface Processes and Landforms, v. 44, p. 27–45, https://doi.org/10.1002/esp.4473.

Seidl, M.A., Dietrich, W.E., and Kirchner, J.W., 1994, Longitudinal profile development into bedrock: An analysis of Hawaiian channels: The Journal of Geology, v. 102, p. 457–474, https://doi.org/10.1086/629686.

Shi, X., 2011, Transient channel incision in response to the Mendocino Triple Junction migration, northern California [M.S. thesis]: University Park, Pennsylvania, The Pennsylvania State University, 82 p.

Shobe, C.M., Tucker, G.E., and Anderson, R.S., 2016, Hillslope-derived blocks retard river incision: Geophysical Research Letters, v. 43, p. 5070–5078, https://doi.org/10.1002/2016GL069262.

Shobe, C.M., Tucker, G.E., and Barnhart, K.R., 2017a, The SPACE 1.0 model: A Landlab component for 2-D calculation of sediment transport, bedrock erosion, and landscape evolution: Geoscientific Model Development, v. 10, p. 4577–4604, https://doi.org/10.5194/gmd-10-4577-2017.

Shobe, C.M., Hancock, G.S., Eppes, M.C., and Small, E.E., 2017b, Field evidence for the influence of wethering on rock erodibility and channel form in bedrock rivers: Earth Surface Processes and Landforms, v. 42, p. 1997–2012, https://doi.org/10.1002/esp.4163.

Shobe, C.M., Tucker, G.E., and Rossi, M.W., 2018, Variable-threshold behavior in rivers arising from hillslope-derived blocks: Journal of Geophysical Research: Earth Surface, v. 123, p. 1931–1957, https://doi.org/10.1029/2017JF004575.

Shobe, C., Bennett, G., Tucker, G., Roback, K., Miller, S., and Roering, J.J., 2020, Figure scripts and data to accompany "Boulders as a lithologic control on river and landscape response to tectonic forcing at the Mendocino Triple Junction": Figshare data set, (available at https://doi.org/10.6084/m9.figshare.11956836.v1).

Sklar, L.S., and Dietrich, W.E., 1998, River longitudinal profiles and bedrock incision models: Stream power and the influence of sediment supply, *in* Tinkler, K.J., and Wohl, E., eds., Rivers Over Rock: Fluvial Processes in Bedrock Channels: Washington, D.C., American Geophysical Union, Geophysical Monograph, v. 107, p. 237–260, doi: https://doi.org/10.1029/GM107p0237.

Sklar, L.S., Riebe, C.S., Marshall, J.A., Genetti, J., Leclere, S., Lukens, C.L., and Merces, V., 2017, The problem of predicting the size distribution of sediment supplied by hillslopes to rivers: Geomorphology, v. 277, p. 31–49, https://doi.org/10.1016/j.geomorph.2016.05.005.

Smith, J.D., 2004, The role of riparian shrubs in preventing floodplain unraveling along the Clark Fork of the Columbia River in the Deer Lodge Valley, Montana, *in* Bennett, S.J., and Simon, A., eds., Riparian Vegetation and Fluvial Geomorphology: Washington, D.C., American Geophysical Union, Water Science and Application Series, Volume 8, p. 71–85, https://doi.org/10.1029/008WSA06.

Snyder, N.P., Whipple, K.X., Tucker, G.E., and Merritts, D.J., 2000, Landscape response to tectonic forcing: Digital elevation model analysis of stream profiles in the Mendocino triple junction region, northern California: Geological Society of America Bulletin, v. 112, p. 1250–1263, https://doi.org/10.1130/0016-7606(2000)112<1250:LRTTFD>2.0.CO;2.

Snyder, N.P., Whipple, K.X., Tucker, G.E., and Merritts, D.J., 2003a, Channel response to tectonic forcing: Field analysis of stream morphology and hydrology in the Mendocino triple junction region, northern California: Geomorphology, v. 53, p. 97–127, https://doi.org/10.1016/S0169-555X(02)00349-5.

Snyder, N.P., Whipple, K.X., Tucker, G.E., and Merritts, D.J., 2003b, Importance of a stochastic distribution of floods and erosion thresholds in the bedrock river incision problem: Journal of Geophysical Research, v. 108, https://doi.org/10.1029/2001JB001655.

Stark, C.P., 2006, A self-regulating model of bedrock channel geometry: Geophysical Research Letters, v. 33, L04402, https://doi.org/10.1029/2005GL023193.

Syvitski, J.P., and Morehead, M.D., 1999, Estimating river-sediment discharge to the ocean: Application to the Eel margin, northern California: Marine Geology, v. 154, p. 13–28, https://doi.org/10.1016/S0025-3227(98)00100-5.

Thaler, E.A., and Covington, M.D., 2016, The influence of sandstone caprock material on bedrock channel steepness within a tectonically passive setting: Buffalo National River Basin, Arkansas, USA: Journal of Geophysical Research: Earth Surface, v. 121, p. 1635–1650, https://doi.org/10.1002/2015JF003771.

Terpilowski, M.A., 2019, scikit-posthocs: Pairwise multiple comparison tests in Python: Journal of Open Source Software, v. 4, p. 1169, https://doi.org/10.21105/joss.01169.

Tucker, G.E., 2004, Drainage basin sensitivity to tectonic and climatic forcing: Implications of a stochastic model for the role of entrainment and erosion thresholds: Earth Surface Processes and Landforms, v. 29, p. 185–205, https://doi.org/10.1002/esp.1020.

Tucker, G.E., and Bras, R.L., 2000, A stochastic approach to modeling the role of rainfall variability in drainage basin evolution: Water Resources Research, v. 36, no. 7, p. 1953–1964, https://doi.org/10.1029/2000WR900065.

Turowski, J.M., 2018, Alluvial cover controlling the width, slope and sinuosity of bedrock channels: Earth Surface Dynamics, v. 6, p. 29–48, https://doi.org/10.5194/esurf-6-29-2018.

Turowski, J.M., Lague, D., and Hovius, N., 2007, Cover effect in bedrock abrasion: A new derivation and its implications for the modeling of bedrock channel morphology: Journal of Geophysical Research: Earth Surface, v. 112, F04006, https://doi.org/10.1029/2006JF000697.

Vallat, R., 2018, Pingouin: Statistics in Python: Journal of Open Source Software, v. 3, p. 1026, https://doi.org/10.21105/joss.01026.

Whipple, K.X., 2004, Bedrock rivers and the geomorphology of active orogens: Annual Review of Earth and Planetary Sciences, v. 32, p. 151–185, https://doi.org/10.1146/annurev.earth.32.101802.120356.

Whipple, K.X. and Tucker, G.E., 1999, Dynamics of the stream-power river incision model: Implications for height limits of mountain ranges, landscape response timescales, and research needs: Journal of Geophysical Research, v. 104, https://doi.org/10.1029/1999JB900120.

Whipple, K.X., and Tucker, G.E., 2002, Implications of sediment-flux-dependent river incision models for landscape evolution: Journal of Geophysical Research: Solid Earth, v. 107, https://doi.org/10.1029/2000JB000044.

Willenbring, J.K., Gasparini, N.M., Crosby, B.T., and Brocard, G., 2013, What does a mean mean? The temporal evolution of detrital cosmogenic denudation rates in a transient landscape: Geology, v. 41, p. 1215–1218, https://doi.org/10.1130/G34746.1.

Wobus, C.W., Tucker, G.E., and Anderson, R.S., 2006a, Self-formed bedrock channels: Geophysical Research Letters, v. 33, L18408, https://doi.org/10.1029/2006GL027182.

Wobus, C., Whipple, K.X., Kirby, E., Snyder, N., Johnson, J., Spyropolou, K., Crosby, B., and Sheehan, D., 2006b, Tectonics from Topography: Procedures, Promise, and Pitfalls: Geological Society of America Special Paper 398, https://doi.org/10.1130/2006.2398(04).

Yanites, B.J., 2018, The dynamics of channel slope, width, and sediment in actively eroding bedrock river systems: Journal of Geophysical Research: Earth Surface, v. 123, p. 1504–1527, https://doi.org/10.1029/2017JF004405.

Yanites, B.J., and Tucker, G.E., 2010, Controls and limits on bedrock channel geometry: Journal of Geophysical Research: Earth Surface, v. 115, F04019, https://doi.org/10.1029/2009JF001601.

Science Editor: Wenjiao Xiao
Associate Editor: Karl Wegmann

Manuscript Received 10 June 2019
Revised Manuscript Received 13 March 2020
Manuscript Accepted 1 June 2020

Printed in the USA